Journal of Catalysis 275 (2010) 84–98

Contents lists available at ScienceDirect

Journal of Catalysis

journal homepage: www.elsevier.com/locate/jcat

Origin of the synergistic interaction between MoO_3 and iron molybdate for the selective oxidation of methanol to formaldehyde

Kamalakanta Routray [a], Wu Zhou [b], Christopher J. Kiely [b], Wolfgang Grünert [c], Israel E. Wachs [a,*]

[a] Operando Molecular Spectroscopy and Catalysis Laboratory, Department of Chemical Engineering, Lehigh University, Bethlehem, PA 18015, USA
[b] Department of Materials Science and Engineering, Lehigh University, Bethlehem, PA 18015, USA
[c] Laboratory of Industrial Chemistry, Ruhr University Bochum, D-44780 Bochum, Germany

ARTICLE INFO

Article history:
Received 26 April 2010
Revised 17 July 2010
Accepted 21 July 2010

Keywords:
Catalysts
Iron molybdate ($Fe_2(MoO_4)_3$)
Oxidation
CH_3OH
HCHO
Spectroscopy
Raman
IR
LEIS
Electron microscopy

ABSTRACT

The origin of the enhanced catalytic performance of bulk iron molybdate catalysts with excess crystalline MoO_3 for methanol oxidation to formaldehyde was investigated with MoO_3, Fe_2O_3, $Fe_2(MoO_4)_3$, MoO_3/$Fe_2(MoO_4)_3$ and model supported MoO_3/Fe_2O_3 catalysts. Low-energy ion scattering (LEIS) analysis of the outermost surface layer revealed that the molybdate catalysts possess a monolayer of surface MoO_x species. Temperature programmed CH_3OH-IR spectroscopy revealed that both intact surface CH_3OH^* and surface CH_3O^* species are present on the catalysts with both yielding HCHO for the redox molybdate catalysts. The addition of excess crystalline MoO_3 to the crystalline $Fe_2(MoO_4)_3$ phase significantly increases the overall steady-state catalytic performance toward HCHO formation. The enhanced catalytic performance of bulk iron molybdate catalysts in the presence of excess MoO_3 is related to the formation of a surface MoO_x monolayer on the bulk $Fe_2(MoO_4)_3$ phase. Thus, the catalytic active phase for bulk iron molybdate catalysts is the surface MoO_x monolayer on the bulk crystalline $Fe_2(MoO_4)_3$ phase and the only role of the excess crystalline MoO_3 is to replenish the surface MoO_x lost by volatilization during methanol oxidation.

1. Introduction

Adkins and Peterson first reported that bulk iron molybdate catalysts are active and selective for methanol oxidation to formaldehyde in 1931 [1]. Bulk iron molybdate catalysts began to be employed as industrial catalysts for oxidation of methanol to HCHO in the 1950s. It has been reported in the catalysis literature, and recognized by the catalyst industry, that the presence of excess crystalline MoO_3 in the bulk iron molybdate catalysts enhances the resulting catalytic performance during selective methanol oxidation reactions [2].

Extensive characterization, catalytic activity and kinetic studies have been undertaken to better understand the catalytic chemistry of excess molybdenum oxide in bulk iron molybdate catalysts. Hill and Wilson investigated the catalyst preparation method for fresh methanol oxidation bulk iron molybdate catalysts containing excess molybdenum oxide with Raman spectroscopy and found that the drying and calcination procedure affected the ratio of crystalline MoO_3 (992 cm^{-1}) and $Fe_2(MoO_4)_3$ (966 cm^{-1}) [3]. Groff was the first to perform *in situ* infrared studies of methanol chemisorption on bulk MoO_3 and found the presence of two surface species: methoxy (CH_3O^*) and intact molecular CH_3OH^* [4]. More recently, Burcham et al. performed similar experiments on MoO_3, Fe_2O_3 and $Fe_2(MoO_4)_3$ catalysts and also found the presence of both surface methoxy species and intact methanol species [5]. The surface methoxy species were dominant on the bulk $Fe_2(MoO_4)_3$ and MoO_3 catalysts and the surface methanol molecular species were more prevalent on the bulk Fe_2O_3 catalyst [5]. Okamoto et al. employed XPS surface analysis to determine the effect of excess molybdenum oxide on the surface composition of bulk iron molybdate catalysts [6]. It was concluded that the presence of excess MoO_3 in Fe_2O_3—MoO_3 catalysts is essential to produce stoichiometric iron molybdate at the catalyst surface, which was thought to be the active phase for the selective oxidation of methanol to formaldehyde. Soares et al. proposed that the active phase of the bulk iron molybdate catalyst has a Mo/Fe = 1.5 ratio and excess MoO_3 is required to replenish the loss of molybdenum oxide from the hot spot region of the reactor [2]. It, thus, appears that the function of excess MoO_3 is to maintain the active phase of the catalyst at the stoichiometric Mo/Fe = 1.5 ratio since the bulk Fe-rich molybdate phase fully oxidizes methanol to CO and CO_2.

Kinetic studies of methanol oxidation over bulk iron molybdate catalysts have demonstrated that the Mars–van Krevelen

* Corresponding author.
E-mail address: iew0@lehigh.edu (I.E. Wachs).

0021-9517/$ - see front matter © 2010 Elsevier Inc. All rights reserved.
doi:10.1016/j.jcat.2010.07.023

mechanism is followed [7]. Machiels et al. performed isotopic oxygen reaction to show that methanol oxidation over $Fe_2(MoO_4)_3$ is redox in nature [8]. House et al. have also observed that the gas phase oxygen is not directly involved in the reaction, but is needed for reoxidizing the catalyst [9]. House et al. studied the diffusion of bulk lattice oxygen to the surface of crystalline $Fe_2(MoO_4)_3$ and found from pulsed CH_3OH studies that the bulk lattice oxygen is only readily available at temperatures above 250 °C [9]. Upon reduction of the bulk $Fe_2(MoO_4)_3$ and MoO_3 phases, bulk α-$FeMoO_4$, MoO_2 and Mo_4O_{11} phases are formed. Machiels et al. found that the oxygen mobility in the bulk lattice of $Fe_2(MoO_4)_3$ is greater than that in bulk MoO_3 since Raman spectroscopy revealed that exposure to $^{18}O_2$ preferentially populated the bulk $Fe_2(MoO_4)_3$ phase [10].

More recently, House et al. examined the activity and selectivity of bulk iron molybdate catalysts for methanol oxidation reactions as a function of Mo/Fe ratios from 0.02 to 4 and found that Mo/Fe ratios greater than 1.5 are required for high catalytic activity and selectivity for formaldehyde [11]. It was concluded that this is a consequence of the need of excess crystalline MoO_3 to replenish the molybdenum oxide volatilized during methanol oxidation at high temperatures. Temperature programmed desorption of methanol from stoichiometric bulk iron molybdate catalysts found that bulk $Fe_2(MoO_4)_3$ is 2–4 times more active than bulk MoO_3 for HCHO formation [12,13]. The increased activity was primarily due to the greater number of exposed catalytic active sites present for isotropic $Fe_2(MoO_4)_3$ than for anisotropic MoO_3 since only the edge sites of crystalline MoO_3 possesses the catalytic active sites [13].

The concept of contact synergy was first put forth to explain the catalytic performance of MoS_2/Co_9S_8 catalysts [14]. It was subsequently extended to explain the activity for bulk $NiMoO_4$, $CoMoO_4$ and $MnMoO_4$ phases in contact with excess crystalline MoO_3 [15–17]. It was proposed that the promotion of one phase occurs at the junction of the two phases (contact potential) that favorably modifies the electronic density of the catalytic active phase. A related theory that has also been proposed in the catalysis literature to account for the synergistic effect of two metal oxide phases in contact during selective oxidation reactions is the remote control theory [18]. According to the remote control theory, the catalyst is composed of two well-defined metal oxide phases, an acceptor phase and a donor phase. The acceptor phase is the center for hydrocarbon activation and can have, when alone, a low catalytic activity for the selective oxidation reaction. The donor phase generally has no selective oxidation activity and its role is to produce activated oxygen at a high rate which spills over to the donor phase, which accelerates in the catalytic cycle. This theory has been applied for bulk Sb_2O_4—MoO_3 catalyst where Sb_2O_4 is the donor phase and MoO_3 is the acceptor phase [19]. According to the remote control theory for methanol oxidation over the bulk iron molybdate catalysts, the excess crystalline MoO_3 phase would act as the donor, which dissociates the gas phase oxygen to atomic oxygen, and supplies the oxygen to the bulk $Fe_2(MoO_4)_3$ phase, which would act as an acceptor and oxidize the methanol molecule to formaldehyde.

The present investigation was undertaken in order to resolve the origin of the enhanced performance of bulk iron molybdate catalysts in the presence of excess MoO_3 for selective oxidation reactions. The catalyst samples employed in the present study were characterized with Raman spectroscopy to determine the bulk and surface metal oxide phases present. The CH_3OH oxidation reaction was selected in the present investigation because of its industrial importance and since it is also a 'smart' chemical probe molecule that can (i) discriminate between different types of surface sites (redox, acid or base) [20,21], (ii) determine the number of exposed catalytic active sites (N_s) [22], (iii) discriminate between the different exposed surface cations (Mo vs. Fe) [5], and (iv) the surface reaction mechanism and kinetics are well understood [23]. The surface chemistry of the MoO_3, Fe_2O_3, $Fe_2(MoO_4)_3$, $MoO_3/Fe_2(MoO_4)_3$ and supported MoO_3/Fe_2O_3 catalysts were chemically probed with *in situ* IR spectroscopy after methanol chemisorption and CH_3OH-temperature programmed surface reaction (TPSR) spectroscopy. The catalytic activity and selectivity of the catalysts were determined by steady-state methanol oxidation reaction at different temperatures, including those corresponding to the industrial reaction temperature. The current findings reveal that the catalytic active sites in bulk iron molybdate catalysts are surface MoO_x species and that the only function of excess crystalline MoO_3 is to replenish the volatilized surface MoO_x species.

2. Experimental

2.1. Catalyst synthesis

The bulk $Fe_2(MoO_4)_3$ catalyst (Mo/Fe = 1.5) was synthesized by co-precipitation of aqueous $Fe(NO_3)_3{\cdot}9H_2O$ (Alfa Aesar Products, 99.9%) and $(NH_4)_6Mo_7O_{24}{\cdot}4H_2O$ (Alfa Aesar Products, 99.9%) precursors. To 200 ml of distilled water, 15 g of ferric nitrate and 20 g of citric acid $(HOC(COOH)(CH_2COOH)_2.H_2O$ Alpha Aesar Products 99.9%) were added and mixed until the complete dissolution of salts. A separate solution of the required amount of ammonium heptamolybdate $(NH_4)_6Mo_7O_{24}{\cdot}4H_2O$ (Alfa Aesar Products, 99.9%) in 200 ml of water was also prepared. Subsequently, the aqueous ammonium heptamolybdate solution was mixed with the aqueous metal-citric acid solution. The mixture was dried at room temperature until a glassy texture was observed. The precursor was further dried at 70 °C overnight, ground and subsequently calcined at 500 °C for 4 h [22,24,25]. The iron molybdate catalysts with excess MoO_3 (Mo/Fe = 1.7 and 2.0) were also prepared by this co-precipitation method. The crystalline MoO_3 phase was prepared by thermal decomposition of $(NH_4)_6Mo_7O_{24}{\cdot}4H_2O$ in air at 400 °C for 6 h. Commercial Fe_2O_3 (Alfa Aesar Products, 99.99%) was calcined at 350 °C in air for 2 h prior to being used as support for the supported MoO_3/Fe_2O_3 catalyst samples. The Fe_2O_3 support was subsequently impregnated with aqueous solutions of the desired amount of ammonium heptamolybdate to yield supported 2.3% and 3% MoO_3/Fe_2O_3 catalysts. After thorough mixing, the samples were dried under ambient conditions for 16 h and calcined in air at 350 °C for 4 h.

2.2. Low-energy ion scattering (LEIS) spectroscopy

The low-energy ion scattering (LEIS) spectra were measured with a Leybold surface analysis system equipped with X-ray and ion sources and an EA 10/100 electron (ion) analyzer with multichannel detection (Specs). The samples were treated in flowing synthetic dry air (20% O_2/N_2) at 723 K for 30 min before they were introduced into the spectrometer vacuum without further contact with the ambient atmosphere.

The LEIS spectra were measured with 2000 eV He^+ ions. The LEIS sputter series were performed by defining narrow scans over the lines of interest and selecting an excitation current low enough to still produce spectra with tolerable noise level. The surface charge was removed with a flood gun. For intensity evaluation, signals were integrated over a Shirley-type background.

2.3. Raman spectroscopy

Raman spectroscopy was performed to examine the metal oxide phases present in the synthesized catalysts. The Raman spectra of bulk MoO_3 and $Fe_2(MoO_4)_3$ (Fe/Mo = 1.5, 1.7 and 2.0) were collected under ambient conditions using a 532nm laser source

[26]. The *in situ* Raman spectra of the dehydrated Fe_2O_3 support and supported 2.3% and 3% MoO_3/Fe_2O_3 catalysts were also obtained. Detailed information about the Raman experimental set-up is provided in the Supplementary material.

2.4. FT-IR spectroscopy

The IR spectra were obtained with an FT-IR spectrometer (SensIR) present on the Horiba-Jobin Yvon LabRam-IR High Resolution spectrometer system. The LabRam-IR spectrometer allowed for the same catalyst spot analysis for Raman and FT-IR. An all-reflecting objective (Cassegrain/Schwarzschild type) was used for the acquisition of the FT-IR signal in the single-beam mode, which allowed displaying of transmittance IR spectra. The mid-IR (400–4000 cm^{-1}) spectra were recorded with an MCT detector at a spectral resolution of 4 cm^{-1} using 100 signal-averaged scans. About ~5–10 mg of loose powder was typically placed in the environmental cell, equipped with a CaF_2 window, to perform *in situ* as well as temperature programmed reaction studies. The procedures for sample pretreatment and exposure to different gaseous environments are described in detail in the CH_3OH-TPSR spectroscopy section below. The IR spectra were collected by using QuaIId-IR software (Version 2) manufactured by SensIR Technologies. The FT-IR spectra presented in this paper were background subtracted with spectra collected at 100 °C under a flowing 10% O_2/He environment. The temperature programmed IR spectroscopy experiments were conducted following the temperature programmed surface reaction spectroscopy procedure, which is described in the Supplementary material. The infrared spectrum of 2.3% MoO_3/Fe_2O_3 was collected in an *in situ* quartz cell with a Nicolet Magna 550 FT-IR spectrometer. The detailed information on the instrument and reaction environment is provided in the Supplementary material.

2.5. High resolution-transmission electron microscopy (HR-TEM)

For TEM analysis, samples were prepared by dipping a lacy carbon TEM grid into the dry catalyst powder and the loosely bound residue was discarded. Bright field (BF) imaging was performed on a JEOL 2000FX TEM operating at 200 kV. Selected area electron diffraction (SAED) analysis and X-ray energy dispersive spectroscopy (XEDS) were also carried out on the same instrument. High resolution TEM (HR-TEM) imaging was performed on a 200 kV JEOL 2200FS (S)TEM having a point-to-point resolution of 0.19 nm in TEM mode [27]. Low electron dose settings were used during electron microscopy characterization in order to minimize electron beam irradiation modification to the samples.

2.6. CH_3OH-TPSR spectroscopy

The CH_3OH-TPSR experiment was used to study the surface chemical kinetics and properties of active sites by employing methanol as a probe molecule. The obtained products HCHO, DME and CO/CO_2 indicate the presence of active redox, acidic and basic sites, respectively, on the surface of the catalyst. The HCHO/CH_3OH-TPSR spectra were further analyzed for surface kinetic information. The first-order Redhead equation was applied to calculate the activation energy, E_a, for HCHO formation. Detailed information about the experimental set-up and procedure was provided in an earlier publication [26].

2.7. Steady-state methanol oxidation

The steady-state methanol oxidation reaction was carried out to determine the catalytic activity and selectivity of the bulk Fe_2O_3, MoO_3, iron molybdate (Mo/Fe = 1.5, 1.7 and 2.0) and supported 2.3% MoO_3/Fe_2O_3 catalysts. The detailed experimental set-up is provided elsewhere [26].

2.8. BET

The BET surface area of the catalyst samples was measured by nitrogen adsorption–desorption in flowing N_2 at −196 °C with a Quantasorb surface area analyzer (Quantachrome Corporation, Model OS-9). A sample quantity of ~0.3 g was typically employed for the measurement, and the sample was outgassed at 250 °C before N_2 adsorption (Quantachrome Corporation, Model QT-3).

3. Results

3.1. BET surface area

The BET surface areas of the bulk MoO_3, Fe_2O_3, stoichiometric $Fe_2(MoO_4)_3$ (Mo/Fe = 1.5), iron molybdates with excess MoO_3 (Mo/Fe = 1.7 and 2.0) and the supported 2.3% MoO_3/Fe_2O_3 catalysts are listed in Table 1. Bulk MoO_3 possess a BET surface area of only a couple of m^2/g and bulk Fe_2O_3 has a modest surface area of 23 m^2/g. The surface area of the supported 2.3% MoO_3/Fe_2O_3 catalyst is also 23 m^2/g. The stoichiometric $Fe_2(MoO_4)_3$ (Mo/Fe = 1.5) compound has a modest BET surface area of 12 m^2/g that decreases by a factor of ~2 for the bulk iron molybdate catalysts containing excess MoO_3 (Mo/Fe = 1.7 and 2.0). Thus, the BET surface area values of the metal oxide catalysts employed in the present investigation are of only modest values (~2–23 m^2/g).

3.2. Low-energy ion scattering (LEIS) spectroscopy

The 3-D LEIS sputtering series plot of the supported 2.3% MoO_3/Fe_2O_3 catalyst is presented in Fig. 1. The very first LEIS scan reveals that the outermost surface layer only possesses Mo species since a Fe signal is not present. The LEIS Fe signal, however, grows with increasing number of sputtering scans because of removal of Mo from the surface by the ion scattering process. The numerical integration gives a finite value for this region, but the extrapolation of the Mo/Fe intensity ratios to zero sputtering time clearly goes through the origin confirming that essentially a complete monolayer was achieved for supported 2.3% MoO_3/Fe_2O_3 catalyst with only surface MoO_x species present in its outermost layer.

The first scan LEIS spectra of the supported 2.3% MoO_3/Fe_2O_3 monolayer and bulk iron molybdate catalysts are presented in

Table 1
BET surface areas, number of active sites (N_s), TPSR T_p values and first-order rate constants, k_{rds}, for HCHO formation for the bulk Fe_2O_3, MoO_3, $Fe_2(MoO_4)_3$, $MoO_3/Fe_2(MoO_4)_3$ and supported MoO_3/Fe_2O_3 catalysts.

Sample (calcination temperature in °C)	BET surface area (m^2/g)	N_s (# of active sites) (μmol/m^2)	T_p (°C)	k_{rds} (s^{-1})
Fe_2O_3 (350)	23	3.0	186 (CH_3OH)	–
1.4 (redox)			189 (HCHO)	0.20
3.4 (acidic)			242 (DME)	–
MoO_3 (400)	2	0.9 (redox)	205 (HCHO)	0.066
Mo/Fe = 1.5 (500)	12	6.1 (redox)	209 (HCHO)	0.050
Mo/Fe = 1.7 (500)	5	14.5 (redox)	190 (HCHO)	0.19
Mo/Fe = 2.0 (500)	5	10.9 (redox)	190 (HCHO)	0.19
2.3% MoO_3/Fe_2O_3 (350)	23	1.6 (redox)	190 (HCHO)	0.19

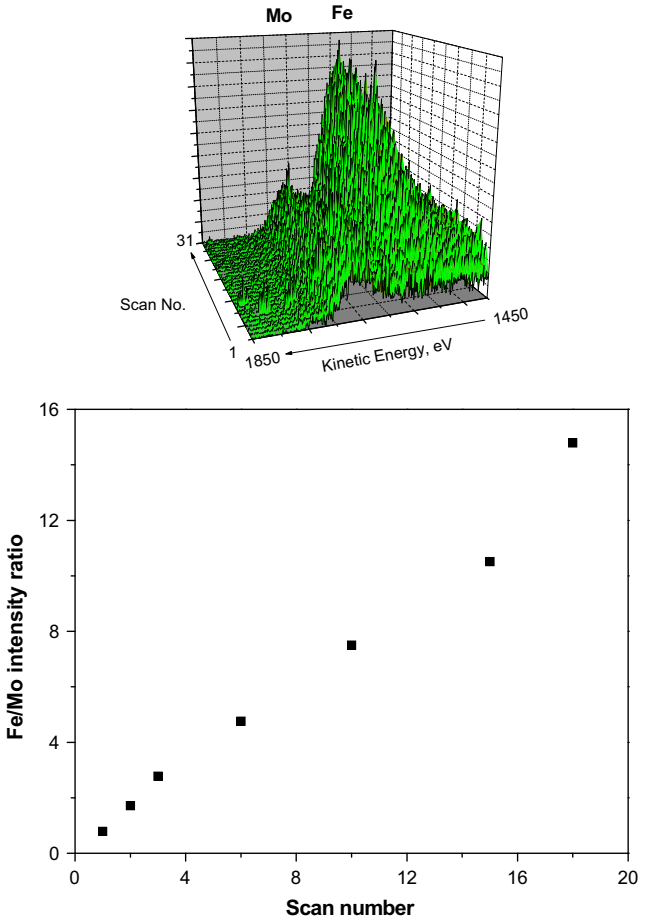

Fig. 1. LEIS spectra of supported 2.3% MoO_3/Fe_2O_3 (a) spectra taken during sputter series, 1 mA sample current and (b) development of Fe/Mo intensity during sputter series.

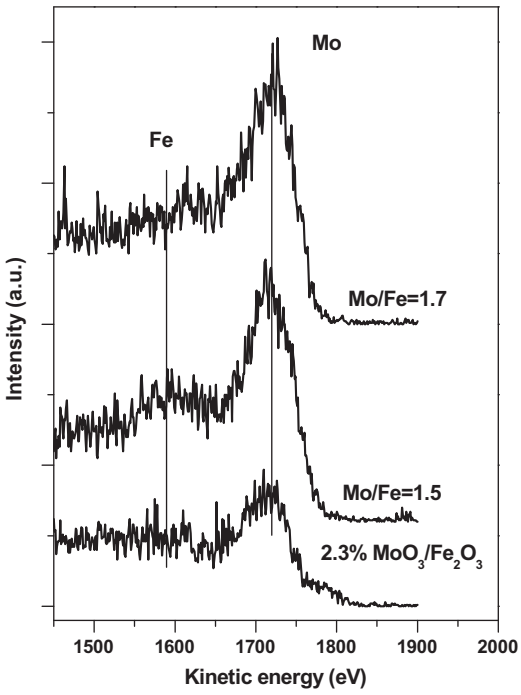

Fig. 2. First scan LEIS spectra of bulk stoichiometric iron molybdate (Mo/Fe = 1.5), Mo/Fe = 1.7 and supported 2.3% MoO_3/Fe_2O_3 catalysts.

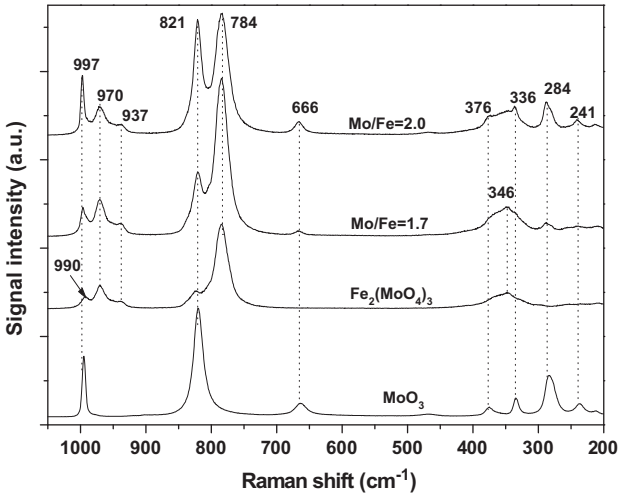

Fig. 3. Raman spectra of ambient MoO_3 and iron molybdate catalysts ($Fe_2(MoO_4)_3$ or Mo/Fe = 1.5, and Mo/Fe = 1.7 and 2.0).

Fig. 2. The 1st LEIS scan reveals the outermost surface layer before sputtering of the surface takes place with increasing number of scans. The 1st LEIS scan for the model supported 2.3% MoO_3/Fe_2O_3 catalyst only exhibits Mo in the outermost surface and is shown for reference. For stoichiometric bulk iron molybdate (Mo/Fe = 1.5), the Fe signal is observed from the very first scan indicating that some exposed Fe sites are present on the outermost surface layer of this catalyst. For bulk iron molybdate with Mo/Fe = 1.7 containing excess MoO_3, only the Mo signal is observed in the first scan and the characteristic Fe signal in the KE region is absent. The 1st scan LEIS spectra demonstrate that excess MoO_3 covers all the exposed Fe sites originally present in the outermost layer of stoichiometric $Fe_2(MoO_3)_3$.

3.3. Raman spectroscopy

The Raman spectra for the bulk MoO_3 and iron molybdates (Mo/Fe = 1.5, 1.7 and 2.0) catalyst samples are presented in Fig. 3. The Raman spectrum of bulk MoO_3 exhibits the characteristic sharp bands of crystalline MoO_3 (997, 821, 666, 376, 336 and 284 cm^{-1}). The Raman band at 997 cm^{-1} originates from the terminal Mo=O symmetric stretch [22,28]. The Raman bands at 200–250 cm^{-1}, 310–370 cm^{-1}, 666 cm^{-1} and 700–850 cm^{-1} of bulk MoO_3 have been assigned to the bridging Mo—O—Mo deformation, bending of terminal Mo=O, symmetric and asymmetric Mo—O—Mo stretching vibrations, respectively [22,28].

The Raman spectrum of bulk $Fe_2(MoO_4)_3$ possesses bands at 336, 784, 821, 937, 970 and 990 cm^{-1}. The bands at 937, 970 and 990 cm^{-1} are the Mo=O symmetric stretches of the three distinct, isolated MoO_4 sites in bulk $Fe_2(MoO_4)_3$ [29]. The Raman bands at 784 and 821 cm^{-1} are the associated asymmetric stretches and the broader band at 336 cm^{-1} is the related bending mode [29]. Note that the weak bands at ~990 and ~937 cm^{-1} and a shoulder at 821 cm^{-1} are associated with the $Fe_2(MoO_4)_3$ phase and are not related to the bulk MoO_3 phase. For the bulk iron molybdate catalysts with excess MoO_3 (Mo/Fe = 1.7 and 2.0), the Raman bands of both crystalline $Fe_2(MoO_4)_3$ and MoO_3 are present with the latter increasing with the Mo/Fe ratio. No evidence for excess crystalline Fe_2O_3 is contained in the Raman spectra suggesting that there was not an excess iron oxide present in the bulk iron molybdate catalysts. The low Raman scattering from the dark Fe_2O_3 phase (see below), however, may not allow detection of small amounts of this

phase [30]. Nevertheless, excess Fe_2O_3 is not expected and the Raman analysis demonstrates that the bulk iron molybdate catalysts were successfully prepared with the two crystalline phases of $Fe_2(MoO_4)_3$ and MoO_3, with the concentration of MoO_3 increasing with molybdenum oxide content above Mo/Fe >1.5. The current Raman findings are in excellent agreement with an earlier publication on the preparation of $Fe_2(MoO_4)_3$—MoO_3 catalysts and demonstrate that the $Fe_2(MoO_4)_3$ (Mo/Fe = 1.5) phase is monophasic and free of excess MoO_3 [3].

Both bulk $Fe_2(MoO_4)_3$ and MoO_3 possess the Raman vibration at ~821 cm^{-1} [24]. The difference between these two bulk phases is reflected by the additional vibrations only unique to bulk MoO_3 (997, 666 and 284 cm^{-1}) and the intensity of these bands relative to those of bulk $Fe_2(MoO_4)_3$ (990, 970, 937, 784 and 336 cm^{-1}). Many Raman studies of bulk $Fe_2(MoO_4)_3$ catalysts incorrectly assign the 990 and 821 cm^{-1} bands to MoO_3 and do not realize that it is also associated with the $Fe_2(MoO_4)_3$ phase [3,31,32]. The 821 cm^{-1} Raman vibration was recently incorrectly assigned to surface MoO_3 species even though the band at 821 cm^{-1} is also associated with the bulk $Fe_2(MoO_4)_3$ phase [31]. The 990 cm^{-1} band was also erroneously assigned to the octahedral MoO_6 present in the amorphous layer of $Fe_2(MoO_4)_3$ and originates from the symmetric stretch of the most distorted MoO_4 site in the bulk $Fe_2(MoO_4)_3$ structure [32]. Since $Fe_2(MoO_4)_3$ does not posses the MoO_3 characteristic peak at 284 cm^{-1}, both the 821 and 990 cm^{-1} peaks are assigned to the $Fe_2(MoO_4)_3$ phase. It is also well documented in the literature that surface MoO_x species typically exhibit broad Raman bands in the ~950–1000 cm^{-1} region under both ambient and *in situ* condition that are distinctly different than the sharp Raman bands of the bulk MoO_3 crystalline phase [33].

The *in situ* Raman spectra of the dehydrated supported 2.3% MoO_3/Fe_2O_3 (4.2 Mo atoms/nm^2) and 3% MoO_3/Fe_2O_3 (5.5 Mo atoms/nm^2) catalysts are presented along with that of the native Fe_2O_3 support in Fig. 4. These two supported MoO_3/Fe_2O_3 catalysts were prepared around the monolayer surface coverage region since previous studies have found that monolayer coverage of surface MoO_x species on oxide supports corresponds to ~4.6 Mo atoms/nm^2 [33–36]. The dehydrated α-Fe_2O_3 support is characterized by sharp bands at 222, 241, 288, 406, 498 and 607 cm^{-1}. Two broad Raman bands at ~818 and ~1099 cm^{-1} are also present for bulk α-Fe_2O_3 that seems to be overtone bands: (607 + 498 ~1099 cm^{-1} and 406 + 406 ~818 cm^{-1}). The Raman spectrum of the dehydrated supported 2.3% MoO_3/Fe_2O_3 (4.2 Mo atoms/nm^2) catalyst is essentially the same as that of the α-Fe_2O_3 support with the exception of a new very weak band at ~724 cm^{-1}, tentatively assigned to the bridging Mo—O—Fe functionality of the surface MoO_x species. Although the Mo=O vibration expected for the surface MoO_x species on Fe_2O_3 support was not detected by Raman spectroscopy against the Fe_2O_3 background in Fig. 4, this Mo=O vibration is present at ~1000 cm^{-1} in the corresponding IR spectrum of the dehydrated supported MoO_3/Fe_2O_3 catalyst and is presented as the inset in Fig. 4. The strong IR band observed at 920 cm^{-1} is assigned to the support Fe_2O_3. The absence of crystalline molybdate Raman bands for the supported 2.3% MoO_3/Fe_2O_3 (4.2 Mo atoms/nm^2) catalyst is consistent with its sub-monolayer coverage of a two-dimensional overlayer of surface MoO_x species on the Fe_2O_3 support. The dehydrated supported 3% MoO_3/Fe_2O_3 catalyst also exhibits the Raman spectrum of the α-Fe_2O_3 support and contains a new small band at ~784 cm^{-1} that is characteristic of bulk $Fe_2(MoO_4)_3$, which indicates that excess MoO_3 reacts with the α-Fe_2O_3 support to form bulk iron molybdate. Thus, only the supported 2.3% MoO_3/Fe_2O_3 catalyst has a bonafide two-dimensional surface MoO_x overlayer approaching monolayer coverage.

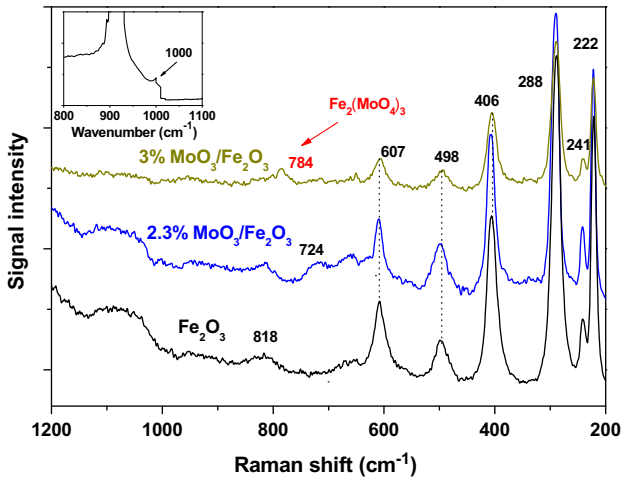

Fig. 4. In situ Raman spectra of dehydrated Fe_2O_3, supported 2.3% (4.2 Mo atoms/nm^2) and 3% MoO_3/Fe_2O_3 (5.5 Mo atoms/nm^2) catalysts. Infrared spectra of 2.3% MoO_3/Fe_2O_3 collected after dehydration at 350 °C (inset).

3.4. Transmission electron microscopy (TEM)

Representative BF and HR-TEM micrographs of $Fe_2(MoO_4)_3$ catalyst are presented in Figs. 5a and 5b, respectively. The images show that bulk iron molybdate consists of aggregates of crystalline particles in the 50–150 nm size range. The lighter contrast regions (4–30 nm in size as indicated in Fig. 5a) indicate that the particles contain internal voids and/or surface pits. Moreover, a 1–2 nm thick amorphous surface overlayer is observed on the bulk $Fe_2(MoO_4)_3$ crystallites. The variations in thickness may be due to the different crystal facet terminations and/or local fluctuations in calcination conditions [37]. Due to the electron beam sensitive nature of mixed oxide materials, low electron dose settings were employed during the HR-TEM image acquisition process. Despite the extreme care taken, the possibility of a small fraction of amorphous layer forming due to electron-beam-induced amorphization can not be ruled out.

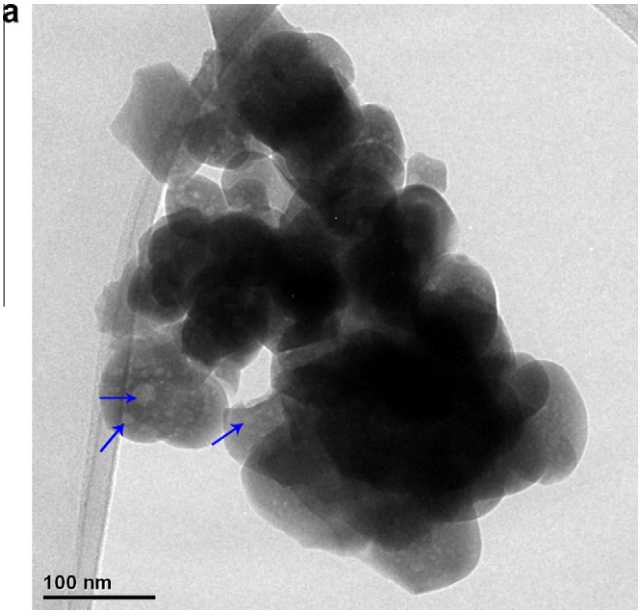

Fig. 5a. Representative BF-TEM micrograph of the bulk $Fe_2(MoO_4)_3$ catalyst.

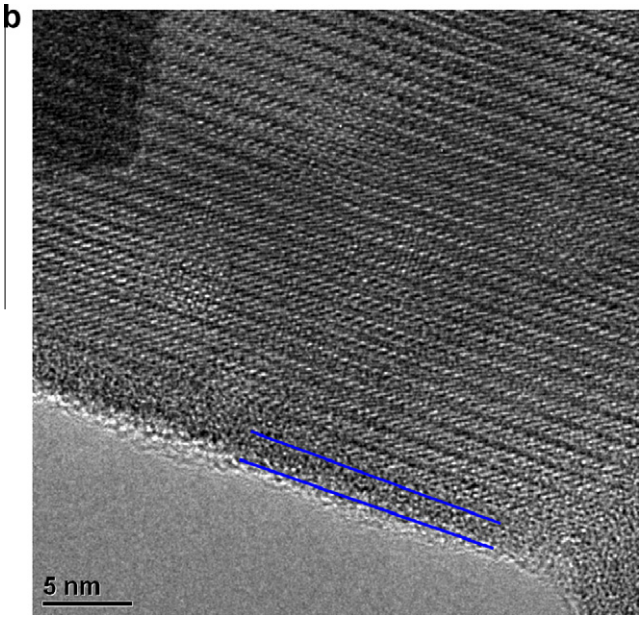

Fig. 5b. Representative HR-TEM micrograph of the bulk $Fe_2(MoO_4)_3$ catalyst showing an amorphous surface layer.

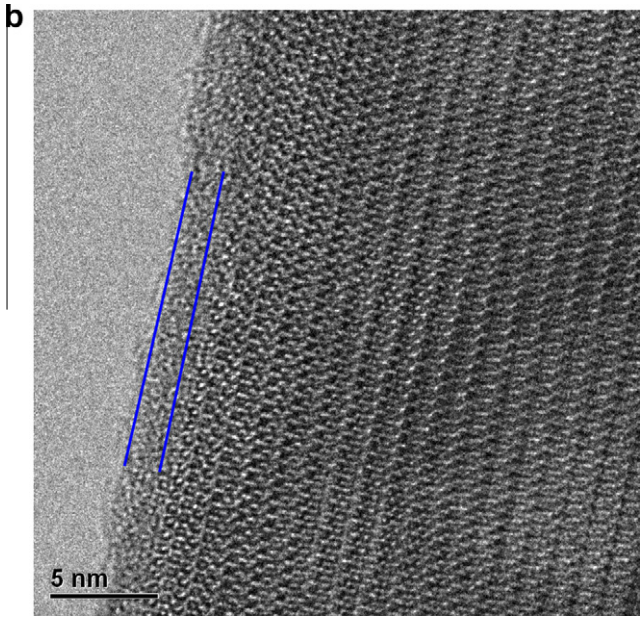

Fig. 6b. Representative HR-TEM image from the majority (X-type) bulk iron molybdate phase present showing an amorphous surface layer.

The BF-TEM and HR-TEM images of the Mo/Fe = 2.0 sample are presented in Figs. 6a and 6b, respectively. The images show the presence of two distinct morphologies. The majority of the sample consists of porous aggregates of particles in the 20–200 nm size range (labeled X). These particles retain their internal voids and/or surface pits as indicated by the 4–30 nm lighter contrast regions in (Fig. 6a). The catalyst particles are similar in morphology to those found in the bulk $Fe_2(MoO_4)_3$ catalyst. Moreover, an amorphous surface overlayer with a 1–2 nm thickness is also observed. Lattice fringe periodicities and intersection angles in the HR-TEM images from these majority type particles can be indexed to the bulk iron molybdate phase as shown in Fig. 6b. XEDS analysis confirms the presence of both Fe and Mo (Fig. 6d) in this X-type morphology. A secondary blade-like morphology (labeled Y) is also observed in Fig. 6a and shown in further detail in Fig. 6c. This morphology consists of large (a few hundred nm) dense particles comprised of multiple stacked well-aligned thin layers as marked by the yellow arrows. Selected area electron diffraction (SAED) patterns from the edge of these particles suggest that all the stacked layers have a common crystal orientation (Fig. S1) and can be indexed to the monoclinic MoO_3 phase. XEDS analysis of the minority phase shows only Mo and O signals, confirming it to be crystalline MoO_3 that originates from direct transformation of the excess MoO_x precursor.

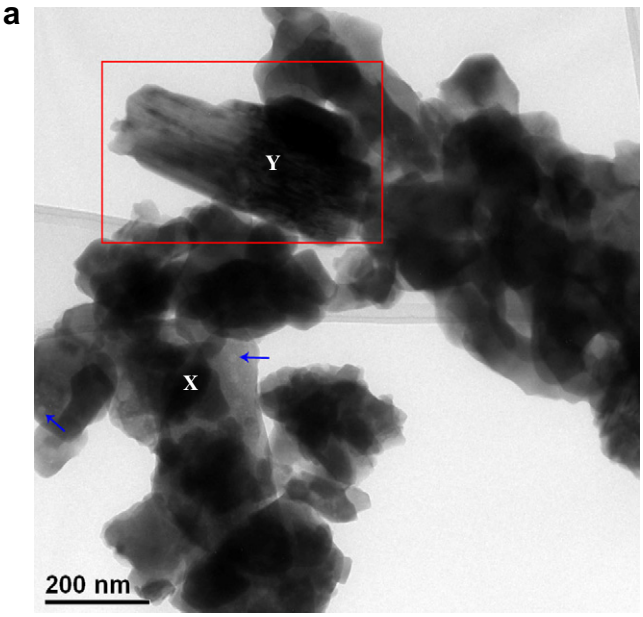

Fig. 6a. Representative BF-TEM image of the bulk iron molybdate (Mo/Fe = 2.0) catalyst.

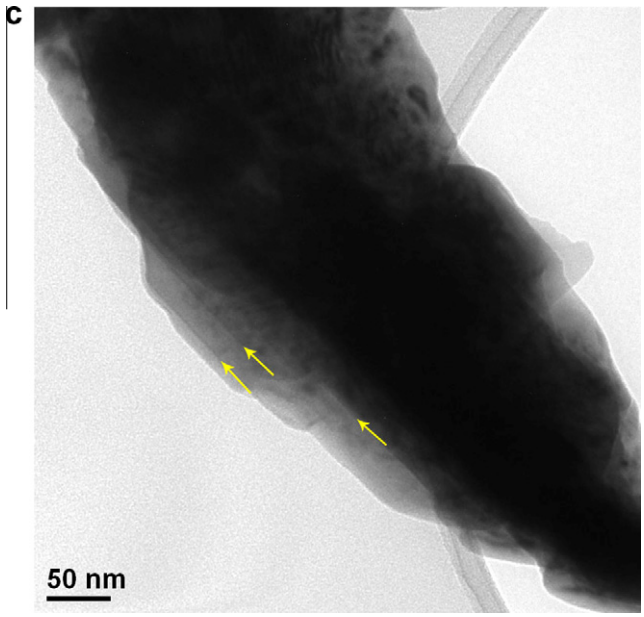

Fig. 6c. A representative BF-TEM image from a minority molybdenum oxide (type-Y type) particle.

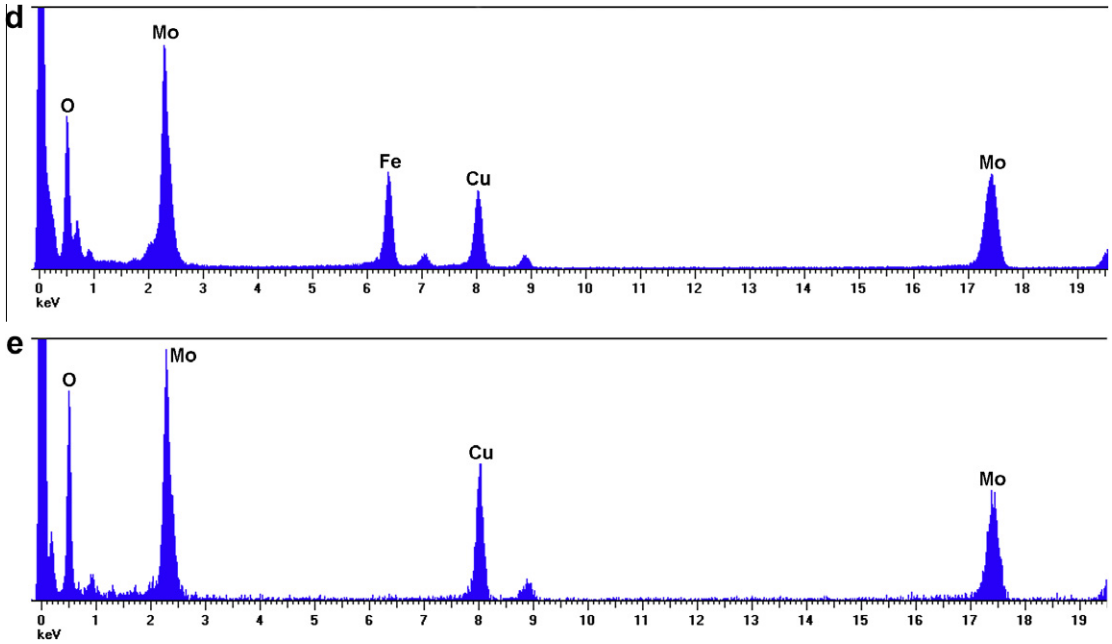

Figs. 6d and e. XEDS spectra from the X-type and Y-type particles, respectively. The Cu peaks in the XEDS spectra are artifacts from the Cu TEM support grid.

Representative BF and HR-TEM images of the supported 2.3% MoO_3/α-Fe_2O_3 model catalyst are presented in Figs. 7a and 7b, respectively. The catalyst consists of agglomerates of plate-like particles having a broad (10–100 nm) particle size distribution (Fig. 7a). Selected area electron diffraction (SAED) analysis of the 2.3% MoO_3/α-Fe_2O_3 model catalyst sample shows diffraction rings corresponding to α-Fe_2O_3 phase only, and no discrete rings corresponding to any crystalline MoO_3 or $Fe_2(MoO_4)_3$ phases were detected. Although the HR-TEM micrograph (Fig 7b) was acquired under identical low electron dose imaging conditions, to those employed for the iron molybdate samples, no obvious surface amorphous layer was observed for the supported 2.3% MoO_3/Fe_2O_3 sample. This suggests that deposited MoO_x is well dispersed on the surface of the crystalline α-Fe_2O_3 support, which is further confirmed by the weak Mo signal in X-ray energy dispersive spectra (XEDS) collected from the sample (Fig. 7c).

3.5. CH_3OH-IR spectroscopy

The *in situ* IR spectra after methanol chemisorption at 100 °C on the bulk MoO_3, Fe_2O_3, $Fe_2(MoO_4)_3$, iron molybdate with excess MoO_3 (Mo/Fe = 1.7 and 2.0) and supported 2.3% MoO_3/Fe_2O_3 catalysts are presented in Fig. 8. The IR spectra prior to CH_3OH adsorption of the dehydrated catalyst sample in the O_2/He environment

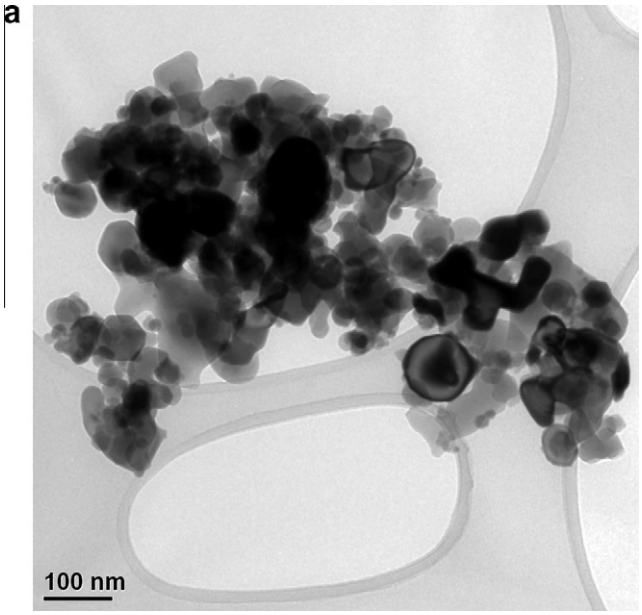

Fig. 7a. Representative BF-TEM micrograph of the model 2.3%MoO_3/α-Fe_2O_3 catalyst

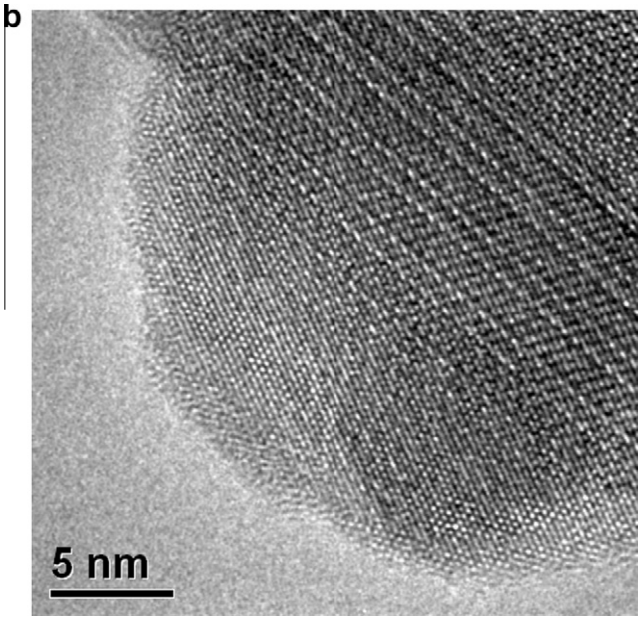

Fig. 7b. HR-TEM micrograph of the model 2.3%MoO_3/α-Fe_2O_3 catalyst.

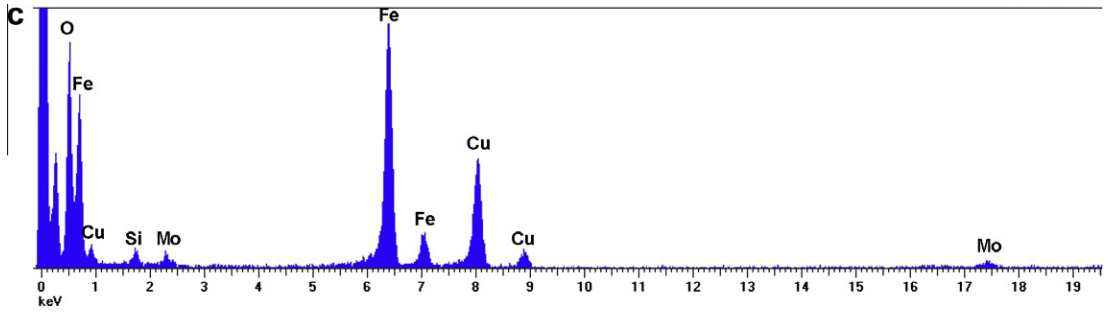

Fig. 7c. An XEDS spectrum from a single catalyst particle ~40 nm in size showing a weak Mo signal. The Cu and Si signals in the XEDS spectrum are artifacts from the Cu TEM grid and EDS detector, respectively.

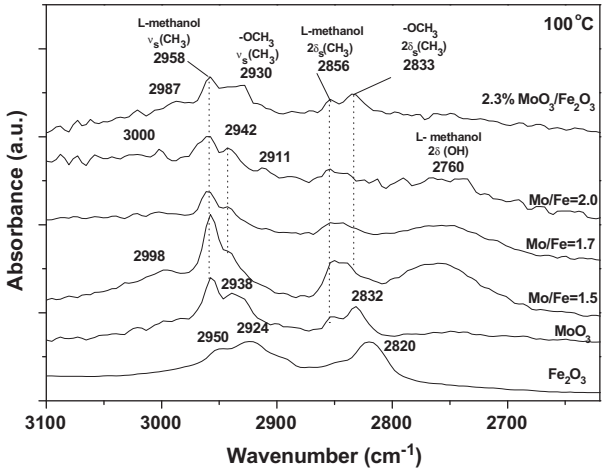

Fig. 8. *In situ* CH_3OH-IR spectra after CH_3OH chemisorption at 100 °C on bulk Fe_2O_3, MoO_3, iron molybdates (Mo/Fe = 1.5 and 1.7, 2.0) and supported 2.3% MoO_3/Fe_2O_3 (containing about a monolayer of surface MoO_x) catalysts.

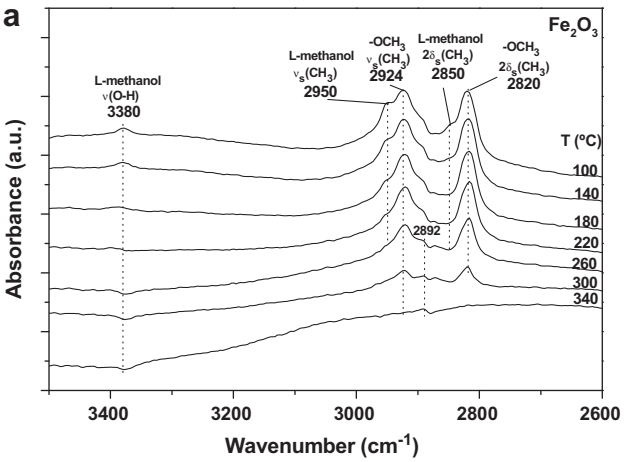

Fig. 9a. CH_3OH-temperature programmed IR spectra from Fe_2O_3.

have been subtracted from that of methanol-exposed surfaces in order to isolate the surface signals resulting from methanol chemisorption.

3.5.1. Bulk Fe_2O_3

Chemisorption of CH_3OH on Fe_2O_3 at 100 °C gives rise to two strong IR peaks at ~2924 and ~2820 cm^{-1} that are characteristic of the C—H stretches for surface methoxy species. Small shoulders also present at ~2950 and ~2850 cm^{-1} originate from the C—H stretches of intact surface CH_3OH species [37]. The CH_3OH-temperature programmed IR spectra from Fe_2O_3 are illustrated in Fig. 9a. The IR bands at 2950 and 2850 cm^{-1} of the intact surface CH_3OH species are shown in Fig. 9a and decrease with increasing temperature and completely disappear at a temperature of 260 °C. The intact surface methanol O—H vibration at 3380 cm^{-1} assigned to ν(O—H) also completely disappears by 260 °C. The disappearance of chemisorbed intact CH_3OH from the Fe_2O_3 surface in the IR spectra corresponds to the appearance of CH_3OH in the gas phase during CH_3OH-TPSR (see Fig. 10a). Thus, the intact surface CH_3OH species is responsible for the appearance of CH_3OH in the gas phase. The IR bands for the surface methoxy species, 2924 and 2820 cm^{-1}, however, only completely disappear above 300 °C and reflect their greater bonding to the Fe_2O_3 surface than the intact surface methanol. The temperature range where the surface methoxy intermediate reacts corresponds to the appearance of gas phase DME during the CH_3OH-TPSR experiment (see Fig. 10a). Thus, the surface methoxy species on Fe_2O_3 react to form DME.

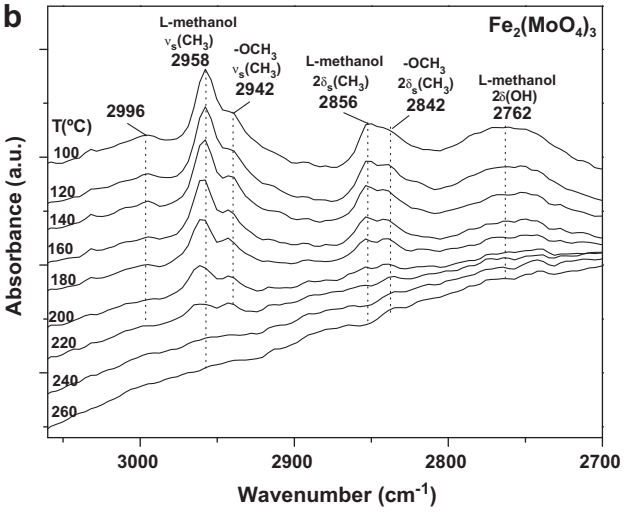

Fig. 9b. CH_3OH-temperature programmed IR spectra for $Fe_2(MoO_4)_3$ (Mo/Fe = 1.5).

3.5.2. Bulk MoO_3

For bulk MoO_3, methanol chemisorption results in IR bands for both intact CH_3OH (2958 and 2856 cm^{-1}) and surface CH_3O^* species (2938 and 2830 cm^{-1}) are shown in Fig. 8, with the intact surface CH_3OH giving rise to a stronger signal.

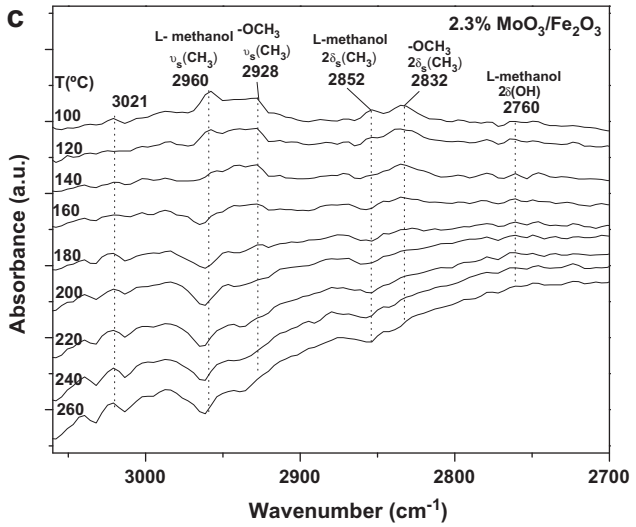

Fig. 9c. CH_3OH-temperature programmed IR spectra from supported 2.3% MoO_3/Fe_2O_3 catalyst.

3.5.3. Bulk iron molybdates (Mo/Fe = 1.5, 1.7 and 2.0)

The IR spectra after CH_3OH chemisorption on the bulk iron molybdate catalysts are shown in Fig. 8 and indicate the presence of intact surface CH_3OH (2958 and 2856 cm^{-1}) and surface methoxy (2942 and 2842 cm^{-1}) species, with the intact surface CH_3OH species being more dominant. Comparison of the CH_3OH IR spectra of the bulk iron molybdates with the corresponding bulk MoO_3 (2958, 2938, 2856 and 2832 cm^{-1}) and Fe_2O_3 (2950, 2924, 2850 and 2820 cm^{-1}) reveals that both the intact surface CH_3OH and surface CH_3O^* are coordinated to the surface Mo oxide sites [5]. The relative intensity of the IR signals for the intact surface CH_3OH and surface methoxy species are also the same for the bulk iron molybdates and MoO_3. The weak IR band at ~2996 cm^{-1} is associated with the ν_{as} (CH_3) of both surface species. The weaker IR intensity for the bulk iron molybdates with Mo/Fe = 1.7 and 2.0 relative to bulk $Fe_2(MoO_4)_3$ (Mo/Fe = 1.5) is related to the significantly lower surface areas of the iron molybdates with excess MoO_3. In summary, the IR spectra for chemisorbed methanol on the bulk iron molybdates indicate that the surface species are primarily coordinated to Mo oxide sites.

The CH_3OH-temperature programmed IR spectra for bulk $Fe_2(MoO_4)_3$ (Mo/Fe = 1.5) are presented in Fig. 9b. As the temperature is increased, the IR bands of the intact surface methanol species (~2958 and ~2856 cm^{-1}) decrease somewhat faster than the vibrations of the surface methoxy species (~2942 and ~2842 cm^{-1}) for the bulk $Fe_2(MoO_4)_3$ catalyst sample. Comparison of the CH_3OH-temperature programmed IR findings with the corresponding CH_3OH-TPSR spectra from bulk $Fe_2(MoO_4)_3$ (see Fig. 10c) reveals that both the surface species are responsible for HCHO formation since only a small amount of CH_3OH is formed from $Fe_2(MoO_4)_3$. Identical CH_3OH-temperature programmed IR spectra were also obtained for the bulk iron molybdates with excess MoO_3 (Mo/Fe = 1.7 and 2.0) and are presented in the Supplementary material. The absence of methanol produced during CH_3OH-TPSR (see Fig. 10c) indicates that the intact surface CH_3OH species are also being converted to HCHO.

3.5.4. Supported 2.3% MoO_3/Fe_2O_3

For the supported MoO_3/Fe_2O_3 catalyst with approximately monolayer coverage of surface MoO_x species on the Fe_2O_3 support, the IR spectrum in Fig. 8 shows that after methanol chemisorption both intact surface CH_3OH (~2958 and 2856 cm^{-1}) and surface methoxy (~2930 and 2833 cm^{-1}) species are present. Note that the IR spectrum is essentially indistinguishable from the corresponding IR spectrum from the bulk MoO_3 catalyst sample. Thus, the CH_3OH IR spectrum of supported MoO_3/Fe_2O_3 demonstrates that the surface of the Fe_2O_3 support is extensively covered by surface MoO_x species. The CH_3OH-temperature programmed IR spectra for the supported 2.3% MoO_3/Fe_2O_3 catalyst are presented in Fig. 9c. With increasing temperature, the intact surface methanol species disappear somewhat faster relative to the surface methoxy species. The intact surface methanol species appears to be gone by ~140 °C. The absence of desorbing CH_3OH from the supported MoO_3/Fe_2O_3 catalyst and the formation of HCHO at this low temperature suggests that the intact surface CH_3OH species are being transformed to surface CH_3O^* species that subsequently react to yield HCHO.

3.6. CH_3OH-temperature programmed surface reaction (TPSR) spectroscopy

TPSR spectroscopy experiments were performed with CH_3OH as the probe molecule to study the surface chemical properties of the

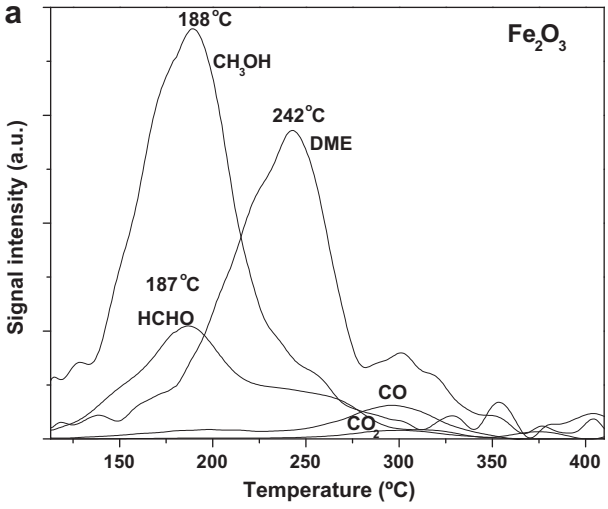

Fig. 10a. CH_3OH-TPSR spectra from bulk Fe_2O_3.

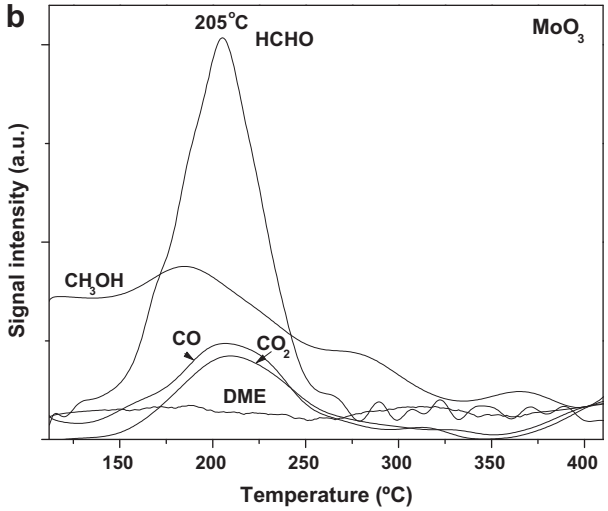

Fig. 10b. CH_3OH-TPSR spectra from bulk MoO_3.

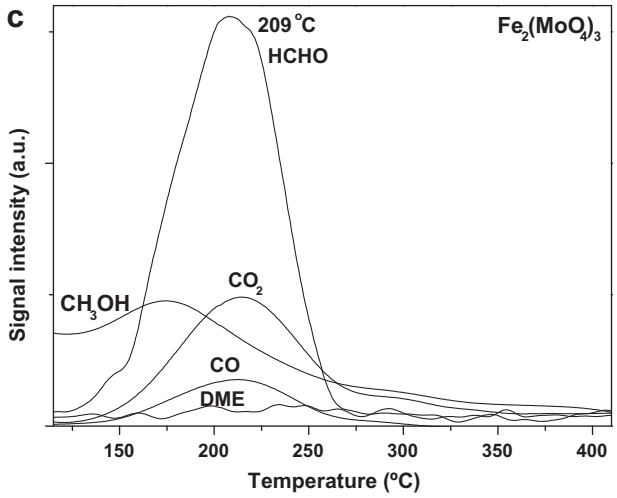

Fig. 10c. CH_3OH-TPSR spectra from bulk $Fe_2(MoO_4)_3$ (Mo/Fe = 1.5).

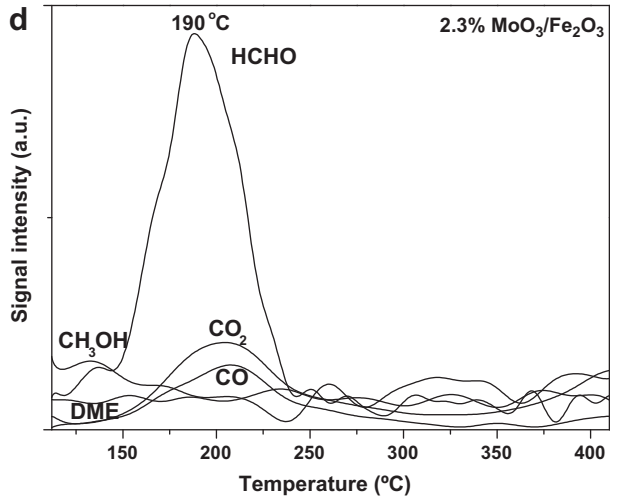

Fig. 10d. CH_3OH-TPSR spectra from supported 2.3% MoO_3/Fe_2O_3 catalyst containing approximately monolayer coverage of surface MoO_x.

metal oxide catalysts. Under reaction conditions, methanol dissociatively chemisorbs to form surface methoxy (CH_3O_{ads}) intermediates. Depending on the nature of the active sites, the surface methoxy intermediate yields either HCHO over redox sites, CH_3OCH_3 over acid sites or CO/CO_2 from basic sites [21]. In addition, CO/CO_2 can also be formed from over-oxidation of HCHO, which must be minimized. The number of each type of catalytic active site can also be determined from the area under the peak of each TPSR spectrum (HCHO, CH_3OCH_3 or CO/CO_2). In addition, the maximum peak temperature is also used to calculate the rate constant, k_{rds}, for the rate-determining-step of the surface reaction.

3.6.1. Bulk Fe_2O_3

The CH_3OH-TPSR spectra from Fe_2O_3 are presented in Fig. 10a. The primary reaction product is DME with T_p value of ~242 °C. In addition, CH_3OH also desorbs with a T_p of ~188 °C. The absence of any significant HCHO and CO/CO_2 formation indicates the low concentration of surface redox and basic sites on Fe_2O_3.

3.6.2. Bulk MoO_3

The CH_3OH-TPSR spectra from bulk MoO_3 are presented in Fig. 10b. The primary reaction product from bulk MoO_3 is HCHO with a T_p value of ~205 °C and almost no desorption of CH_3OH is observed. The absence of any significant DME from acid sites and CO/CO_2 from basic sites indicates that the surface of MoO_3 mainly consists of redox sites. Similar T_p value has been observed for MoO_3 by other groups under UHV experiments [38].

3.6.3. Bulk $Fe_2(MoO_4)_3$ (Mo/Fe = 1.5)

The CH_3OH-TPSR spectra from bulk $Fe_2(MoO_4)_3$ are presented in Fig. 10c. The primary product is HCHO with a T_p value of ~209 °C and only small amounts of CH_3OH also desorbed with a T_p value of ~165 °C. The absence of DME and CO/CO_2 formation reflects the redox nature of the surface of bulk $Fe_2(MoO_4)_3$. Comparison of the CH_3OH-TPSR results for bulk MoO_3, Fe_2O_3 and $Fe_2(MoO_4)_3$ reveals that the surface chemistry of the stoichiometric $Fe_2(MoO_4)_3$ is dominated by that of molybdenum oxide and not iron oxide.

3.6.4. Bulk iron molybdates (Mo/Fe = 1.7 and 2.0)

The CH_3OH-TPSR spectra from the bulk iron molybdates with excess MoO_3 (Mo/Fe = 1.7 and 2.0) are presented in the Supplementary section since they are similar to that of bulk $Fe_2(MoO_4)_3$. The HCHO T_p value, however, shifts from 209 to 190 °C reflecting the presence of slightly more active catalytic sites when excess MoO_3 is present in the bulk iron molybdate catalysts. In addition, the amount of desorbed CH_3OH also completely diminishes in the presence of excess MoO_3.

3.6.5. Supported MoO_3/Fe_2O_3

The CH_3OH-TPSR spectra for the supported 2.3% MoO_3/Fe_2O_3 catalyst are shown in Fig. 10d. Similar to the other Mo-containing catalysts, only HCHO is produced from surface redox sites. The absence of any DME formation reveals that the surface acidic sites of Fe_2O_3 are extensively covered by the redox surface MoO_x sites. The HCHO T_p value is ~190 °C, which is the same that was obtained with iron molybdate catalysts with excess MoO_3. This suggests that similar catalytic active sites are present for the supported MoO_3/Fe_2O_3 and $MoO_3/Fe(MoO_4)_3$ catalysts.

3.6.6. Mars–van Krevelen mechanism

To check for the participation of lattice oxygen in methanol oxidation, cyclic HCHO/CH_3OH-TPSR experiments where the stoichiometric $Fe_2(MoO_4)_3$ catalyst was not oxidized between the TPSR experiments were undertaken and the results are presented in Fig. 11. Note that the HCHO T_p values remain essentially the same

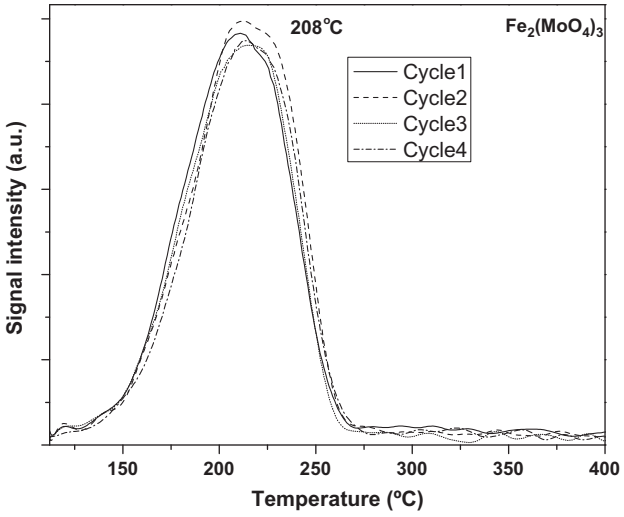

Fig. 11. Cyclic HCHO/CH_3OH-TPSR spectra from the bulk $Fe_2(MoO_4)_3$ (Mo/Fe = 1.5) catalyst (the catalyst was not oxidized between the TPSR experiments).

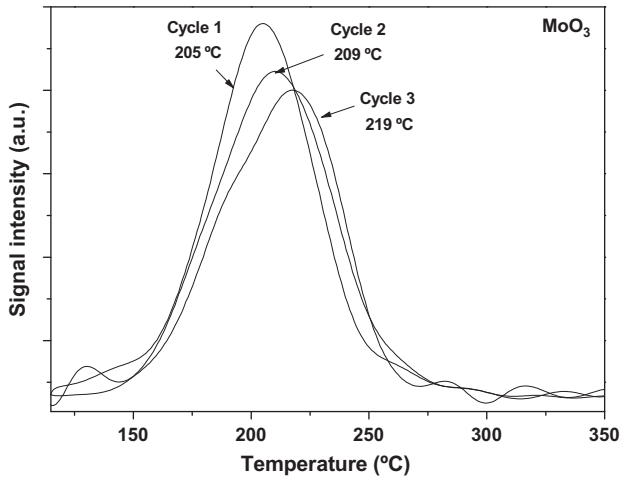

Fig. 12. Cyclic HCHO/CH_3OH-TPSR spectra from bulk MoO_3 catalyst (the catalyst was not oxidized between the TPSR experiments).

as the bulk $Fe_2(MoO_4)_3$ phase is progressively reduced by CH_3OH in each TPSR cycle. The constant T_p value for the HCHO/CH_3OH-TPSR experiments demonstrates that the bulk $Fe_2(MoO_4)_3$ catalyst indeed operates via a Mars–van Krevelen mechanism where the surface cations are being reoxidized by bulk lattice oxygen. The cyclic HCHO/CH_3OH-TPSR experiments for the bulk MoO_3 are presented in Fig. 12. The figure shows that the T_p values increases and peak area decreases with the number of cycles. The increasing T_p value suggests that the oxidation state of surface MoO_3 decreases with the cyclic adsorption of methanol. The decreasing area of the curve suggests that the number of active sites is reduced with each cycle of adsorption. This may be attributed to the fact that the diffusion of lattice oxygen from the bulk to surface is a slow process and therefore, unable to oxidize all the reduced MoO_3 present on the surface. This shows that Mars–van Krevelen mechanism is only sluggishly followed by the MoO_3 catalyst. This contrasts with the $Fe_2(MoO_4)_3$ study where the bulk oxygen readily diffuses to the surface and oxidizes the reduced MoO_x species. Thus, the bulk $Fe_2(MoO_4)_3$ phase is the only bulk metal oxide catalyst component that truly operates by the Mars–van Krevelen mechanism that involves rapid diffusion of bulk lattice oxygen to the catalyst surface.

3.6.7. N_s (number of active sites/m^2)

The number of surface sites per m^2 for the bulk and supported metal oxide catalysts were determined by integrating the HCHO/CH_3OH-TPSR spectra and are listed in Table 1. Bulk MoO_3 contains ~0.9 μmol/m^2 of active sites. The significantly lower value of bulk MoO_3 is related to the anisotropic morphology of this oxide and the preferential chemisorption of methanol at the edge sites of the platelets [13]. The stoichiometric $Fe_2(MoO_4)_3$ phase is isotropic and possesses a surface density ~6.1 μmol/m^2 of active sites. Introducing excess MoO_3 to the bulk iron molybdate catalysts increases the surface density of active sites. The surface density of number of surface active sites significantly decreases when the surface MoO_x monolayer is introduced onto the Fe_2O_3 support, but the nature of the surface sites also change from acidic to redox.

3.6.8. First-order rate constants (k_{rds}) for HCHO formation

The first-order rate constants for surface methoxy decomposition to HCHO were determined by application of the Redhead equation using the TPSR T_p values and are also listed in Table 1. The relative surface kinetics for surface methoxy decomposition by the redox surface sites varies by a modest factor of ~4 for the redox molybdate catalysts as follows: $MoO_3/Fe_2O_3 \sim MoO_3/Fe_2(MoO_4)_3 > Fe_2(MoO_4)_3 \sim MoO_3$.

Table 2
Steady-state catalytic activity of iron molybdate catalysts at 230 and 300 °C (CH_3OH/O_2/He = 6/13/81; total flow rate = 100 ml/min) under differential reaction conditions.

Sample	T (°C)	Selectivity (%)			Overall rate (μmol/m^2 s)	TOF_{Redox} (s^{-1})
		HCHO	DME	DMM		
Fe_2O_3	230	0	70	30	0.7	0.0
	300	48	51	1	8.2	–
MoO_3	–	–	–	–	–	–
	300	65	20	15	4.4	–
Mo/Fe = 1.5	230	73	15	12	0.8	0.09
	300	75	22	3	6.3	0.77
Mo/Fe = 1.7	230	80	8	12	3.2	0.12
	300	87	10	3	23.8	0.94
Mo/Fe = 2.0	230	81	8	11	2.6	0.12
	300	88	9	3	16.3	0.86
2.3% MoO_3/Fe_2O_3	230	80	20	0	0.9	0.44
	300	95	5	0	9.3	5.6

3.7. Steady-state CH_3OH oxidation

The steady-state CH_3OH oxidation over bulk and supported iron molybdate catalysts was performed at 230 and 300 °C and is presented in Table 2. The amount of catalyst was varied so as to keep the conversion between 8% and 18% to maintain differential reaction conditions [39]. Note that CO and CO_2 are essentially not formed indicating that basic surface sites on these iron molybdate catalysts are minimally present. The turnover frequency (TOF) values, defined as the methanol conversion reaction rate per catalytic active surface redox site, are also presented in Table 2. The number of catalytic active redox sites was obtained from the CH_3OH-TPSR experiments and is presented in Table 1. The TOF_{redox} is obtained by multiplying the HCHO selectivity with the overall TOF.

The bulk Fe_2O_3 catalyst is highly selective toward DME formation, which reflects the acidic nature of the surface FeO_x sites. The formation of DMM indicates the presence of surface redox sites since HCHO is required for the formation of DMM [40]. The bulk MoO_3 predominately exhibits surface redox character with some surface acid character also present. All the iron molybdate catalysts (Mo/Fe = 1.5, 1.7 and 2.0) are highly selective toward HCHO showing the surface redox nature of these catalysts. The higher TOF value of 2.3% MoO_3/Fe_2O_3 demonstrates that only surface MoO_x species on Fe_2O_3 are needed for efficient iron molybdate for methanol oxidation to formaldehyde.

3.7.1. TOF_{redox}

The TOF_{redox} values for methanol oxidation to formaldehyde were calculated for the 230 °C since the methanol conversions were between 8% and 18% and satisfied differential reaction conditions. The acidic Fe_2O_3 catalyst did not yield any HCHO product. The TOF_{redox} values for the molybdate catalysts varied from ~0.01 to 0.94 s^{-1}. The much higher TOF_{redox} values for the iron molybdate catalysts than that for bulk MoO_3 reflects the positive synergistic interactions between molybdenum oxide and iron oxide. The essentially identical TOF_{redox} values for the bulk $Fe_2(MoO_4)_3$ and $MoO_3/Fe_2(MoO_4)_3$ catalysts reveal that there is no synergistic interaction between the crystalline MoO_3 and $Fe_2(MoO_4)_3$ phases.

4. Discussion

4.1. CH_3OH surface reaction mechanism

IR spectroscopy has demonstrated that both intact surface CH_3OH^* and CH_3O^* species are present on iron molybdate catalysts [5]. The intact surface CH_3OH^* species are associated with surface

Lewis acid sites and surface CH_3O^* species are present on less acidic or basic surface sites. The surface methoxy species predominate on Fe_2O_3 and the intact surface CH_3OH^* species are the major surface species on Mo oxide containing catalysts. On the surface of Fe_2O_3, the intact surface CH_3OH^* species desorb as molecular CH_3OH and the surface methoxy species react to form CH_3OCH_3. On the iron molybdate surfaces, however, both the intact surface CH_3OH^* and surface CH_3O^* mostly undergo reaction to HCHO. The different reaction pathways are related to the availability of lattice oxygen for the iron molybdate catalysts, which is further elaborated on below.

On the Fe_2O_3 surface, which contains few redox sites, the following reaction mechanism primarily takes place during methanol oxidation:

$$CH_3OH + * \rightarrow CH_3OH^* \quad (1)$$
$$CH_3OH + O^* + * \Longleftrightarrow CH_3O^* + OH^* \quad (2)$$
$$CH_3OH^* \rightarrow CH_3OH + * \quad (\text{rds}) \quad (3)$$
$$CH_3O^* + * \rightarrow CH_3^* + O^* \quad (\text{rds}) \quad (4)$$
$$CH_3^* + CH_3O^* \Longleftrightarrow CH_3OCH_3 \quad (5)$$
$$HO^* + OH^* \Longleftrightarrow H_2O + O^* \quad (6)$$
$$O_2 + 2^* \Longleftrightarrow 2O^* \quad (7)$$

with * representing an empty surface site, X^* representing a surface bound intermediate, rds referring to rate-determining-step, and surface O^* being supplied by dissociation of gas phase molecular O_2. The inability of bulk Fe_2O_3 to readily supply lattice O^* is responsible for the minimal amount of HCHO produced and the significant production of CH_3OCH_3 and CH_3OH reaction products.

For the iron molybdate catalysts, which contain a high concentration of surface redox molybdate sites, surface O^* can be supplied from both lattice and gas phase molecular oxygen. The ready availability of surface O^* is responsible for conversion of both the intact surface CH_3OH^* and CH_3O^* to HCHO via the following reaction mechanism during methanol oxidation:

$$CH_3OH + * \rightarrow CH_3OH^* \quad (8)$$
$$CH_3OH + O^* + * \Longleftrightarrow CH_3O^* + OH^* \quad (9)$$
$$CH_3OH^* \rightarrow CH_3OH + * \quad (10)$$
$$CH_3OH^* + O^* \rightarrow HCHO + H_2O + * \quad (\text{rds}) \quad (11)$$
$$CH_3O^* + O^* \rightarrow HCHO + HO^* \quad (\text{rds}) \quad (12)$$
$$CH_3O^* + HO^* \Longleftrightarrow CH_3OH + O^* + * \quad (13)$$
$$HO^* + OH^* \Longleftrightarrow H_2O + O^* \quad (14)$$
$$O^*_{\text{bulk lattice}} \Longleftrightarrow O^* \quad (15)$$
$$O_2 + 2^* \Longleftrightarrow 2O^*_{\text{bulk lattice}} \quad (16)$$

The absence of CH_3OCH_3 formation reflects the ready availability of surface O^* for redox reactions. The production of minor amounts of CH_3OH is both from desorption of intact surface CH_3OH^* and the hydrogenation of surface CH_3O^* by the hydrogen generated by surface methoxy decomposition to formaldehyde [42]. The formation of carbon oxides arises from basic surface sites and readsoprtion of HCHO that leads to surface formate ($HCOO^*$) species.

4.2. Mars–van Krevelen mechanism

The bulk iron molybdate catalysts function by a Mars–van Krevelen mechanism that employs bulk lattice O^*. This was demonstrated by performing several CH_3OH-TPSR cycles without intermediate catalyst reoxidation (see Fig. 11). The constant T_p value during the CH_3OH-TPSR cycles for bulk $Fe_2(MoO_4)_3$ clearly reveals that the surface sites remain fully oxidized by oxygen being supplied from the bulk lattice oxygen. The area under the CH_3OH-TPSR curves also remains constant reflecting complete reoxidation of the surface sites by bulk lattice oxygen. Machiels and Sleight also observed that the Mars–van Krevelen mechanism is followed over bulk iron molybdate catalysts [8].

Parallel CH_3OH-TPSR experiments with bulk MoO_3, however, show an increase in T_p with increasing number of CH_3OH-TPSR cycles. This suggests that the oxidation state of MoO_3 surface decreases during the CH_3OH-TPSR cycles [43]. The reduction in the area under the HCHO/CH_3OH-TPSR curves further reveals that all the surface MoO_x sites are not being reoxidized by bulk lattice oxygen. Thus, bulk MoO_3 only sluggishly follows the Mars–van Krevelen mechanism due to the slower diffusion of its bulk lattice oxygen. The same effects have been observed by Machiels et al. employing CH_3OH pulses where it was observed that the diffusion of bulk lattice oxygen is slow for MoO_3 compared to $Fe_2(MoO_4)_3$ [10]. Consequently, the bulk MoO_3 phase is not the catalytic active phase in bulk iron molybdate catalysts containing excess MoO_3 and, thus, the catalytic active phase is associated with bulk $Fe_2(MoO_4)_3$.

4.3. Kinetics and selectivity

Under reaction temperatures [44], the surface concentration of CH_3OH^* is low and the rate of methanol oxidation to formaldehyde can be simplified to:

$$r = k_{\text{rds}} K_{\text{ads}} P_{CH_3OH} N_s \quad (17)$$

with k_{rds} representing the first-order rate constant (s^{-1}), K_{ads} the methanol adsorption equilibrium constant (atm^{-1}), P the partial pressure of methanol (atm) and N_s the surface density of redox sites ($\mu mol/m^2$).

For the molybdate catalysts, the methanol oxidation reaction rate is independent of molecular O_2 partial pressure, zero-order dependence, because the surface O^* involved in the rds is being supplied by the bulk lattice oxygen (Mars–van Krevelen reaction mechanism). The first-order rate constants, k_{rds}, for surface methoxy decomposition vary only modestly by a factor of ~4 among the molybdate catalysts indicating that this surface reaction step is not a significant variable among the molybdate catalysts. The TOF_{redox}, $TOF_{\text{redox}} = k_{\text{rds}} K_{\text{ads}} P_{CH_3OH}$, also varies only modestly among the iron molybdate catalysts and reflects the positive interaction between molybdenum oxide and iron oxide to result in active and selective catalysts. The kinetic variations in differential TOF_{redox} and k_{rds} among the iron molybdate catalysts are not significant and demonstrate that the enhanced performance of the $MoO_3/Fe_2(MoO_4)_3$ catalysts relative to $Fe_2(MoO_4)_3$ has primarily to do with the improved selectivity brought about by covering the acidic surface FeO_x sites with the redox surface MoO_x sites.

The Raman spectrum of the supported 2.3% MoO_3/Fe_2O_3 catalyst did not provide surface information because of the strong signal from the Fe_2O_3 support. Infrared spectroscopy, however, exhibited a Mo=O vibration at ~1000 cm^{-1} characteristic of surface MoO_x species. Surface MoOx species can possess one or two terminal Mo=O bonds and their vibrations occur at 1000–1040 cm^{-1} and 960–990 cm^{-1}, respectively [45]. Thus, the IR band at ~1000 cm^{-1} is assigned to mono-oxo surface $O{=}MoO_4$ species since it is the most stable structure of molybdenum oxide under dehydrated conditions [46,47].

Although the synergistic interaction between molybdenum oxide and iron oxide is responsible for the enhanced performance of the supported MoO_3/Fe_2O_3 catalyst system, the TOF_{redox} value for methanol oxidation over the supported MoO_3/Fe_2O_3 system is comparable to other supported molybdenum oxide catalysts [35]. Unlike the supported vanadium oxide catalysts where the TOF_{redox} varies strongly with the oxide support [41], the TOF_{redox} of the supported molybdenum oxide catalysts do not vary much with the oxide support [35].

4.4. Surface density of exposed surface redox sites (N_s)

The HCHO/CH_3OH-TPSR spectra were employed to count the number of exposed surface redox catalytic active sites/m^2. The plate-like crystal structure of anisotropic MoO_3 primarily exposes the basal ⟨0 1 0⟩ plane and to a lesser extent the side ⟨1 0 0⟩ and ⟨1 0 1⟩ planes [48]. The edge planes typically represent ~10% of total MoO_3 surface area and contribute toward the methanol oxidation [49]. The surface MoO_x sites at the edges possess a lower coordination number and preferentially dissociatively chemisorb CH_3OH and are the active sites for methanol adsorption and oxidation [44]. The basal ⟨0 1 0⟩ plane consists of exposed terminal Mo=O sites that have been found to be relatively inactive for CH_3OH dissociative chemisorption as well as methanol oxidation. In contrast, bulk $Fe_2(MoO_4)_3$ is isotropic and all the exposed planes can dissociatively chemisorb CH_3OH as well as oxidize methanol to formaldehyde, which increase the surface density of the number of active sites by a factor of ~6 (see Table 1 and Ref. [12]).

The surface of bulk $Fe_2(MoO_4)_3$ is enriched in surface MoO_x redox sites since HCHO is the predominant reaction product during CH_3OH-TPSR and steady-state methanol oxidation. The surface enrichment of redox MoO_x sites for bulk $Fe_2(MoO_4)_3$ was also previously demonstrated with *in situ* CH_3OH-IR chemisorption studies [5]. The formation of some DME during steady-state methanol oxidation suggests that exposed surface FeO_x sites or even possibly acidic MoO_x sites are also present for bulk $Fe_2(MoO_4)_3$ catalysts, especially during steady-state methanol oxidation where MoO_x can be volatilized by the formation of gaseous Mo—OCH_3 complexes [24,50]. Introduction of excess MoO_3 to $Fe_2(MoO_4)_3$ catalysts further increases the surface density of surface redox sites by as much as a factor of ~2.5, which is ~15 times that for bulk MoO_3 (see Table 1). The increase in the surface active site density with increase in MoO_3 is most probably accentuated because of the error associated in measuring small surface areas. Machiels et al. also found that HCHO selectivity of bulk $Fe_2(MoO_4)_3$ catalysts slightly increased with addition of excess MoO_3 [51]. In the industrial methanol oxidation process, the pelletized catalyst present in the top or hot spot region of the reactor bed preferentially lose the MoO_3 component leaving behind the $Fe_2(MoO_4)_3$ component. The volatilized MoO_3 gets deposited on the catalysts present in colder region of the reactor bed [25]. This deactivation decreases the activity and selectivity of the catalytic reactor. The deactivated catalysts can be regenerated by exposing them to a stream of methanol—He at 250–400 °C since the Mo—CH_3O species are mobile, which uniformly spreads the remaining crystalline MoO_3 present in the interior portion of the catalyst pellet [24]. Thus, as shown in Fig. 13, the role of excess MoO_3 in bulk $Fe_2(MoO_4)_3$ catalysts is to act as a reservoir that can supply surface MoO_x species to cover up exposed surface FeO_x sites and also increase the surface density of redox sites.

4.5. Nature of catalytic active site in bulk iron molybdate catalysts

The bulk $Fe_2(MoO_4)_3$ phase is the catalytic active phase of iron molybdate catalysts since, unlike the bulk MoO_3 phase, it is able to readily operate via the Mars–van Krevelen mechanism and also possesses a high surface density of surface redox sites. The catalytic active redox sites, however, are the surface MoO_x species on the surface of the bulk $Fe_2(MoO_4)_3$ phase. This is further supported by the presence of an amorphous layer of ~1 nm thickness for stoichiometric $Fe_2(MoO_4)_3$, shown in Fig. 5a, and surface MoO_x enrichment for bulk $MoO_3/Fe_2(MoO_4)_3$ as found with LEIS surface analysis. Furthermore, the surface MoO_x overlayer on the Fe_2O_3 support nicely demonstrates that the acidic surface sites of Fe_2O_3 become titrated by the redox surface MoO_x species making the resulting catalyst become almost exclusively redox in nature. Somewhat surprisingly, the HCHO selectivity of the supported MoO_3/Fe_2O_3 catalyst is even higher than that of the bulk iron molybdate catalysts. This trend may reflect the differences between surface MoO_x coordinated to the $Fe_2(MoO_4)_3$ and Fe_2O_3 supports. Thus, the surface MoO_x species on bulk $Fe_2(MoO_4)_3$ are the catalytic active sites in bulk iron molybdate mixed metal oxide catalysts.

Previous literature studies of methanol oxidation to formaldehyde over bulk iron molybdate catalysts have proposed the formation of the reduced α-$FeMoO_4$ phase at lower temperatures and β-$FeMoO_4$ phase at temperatures greater than 310 °C [9,52–54]. A recent study employing ultra-rapid *in situ* X-ray diffraction technique demonstrated that the reduction of $Fe_2(MoO_4)_3$ with H_2, in the absence of O_2, at 420 °C was a slow process and even incomplete after 30 min of exposure to the reducing environment [55]. The reoxidation process, however, was found to be very rapid and complete within 15 s of exposure to O_2. This indicates that reoxidation is more than 100 times faster than reduction. Furthermore, it is important to keep in mind that the methanol oxidation reaction over bulk iron molybdate catalysts is conducted in excess oxygen ($O_2/CH_3OH \sim 2$). Thus, the oxidation kinetics is extremely faster than the reduction kinetics and the presence of the reduced iron molybdate phases such as $FeMoO_4$ phases are highly unlikely [55]. This is consistent with XRD studies demonstrating that the bulk $FeMoO_4$ phase is not present during steady-state methanol oxidation and can only be formed after extensive reduction with methanol [9]. Furthermore, these bulk diffraction measurements are bulk techniques and, therefore, do not provide information about the state of the surface catalytic active sites.

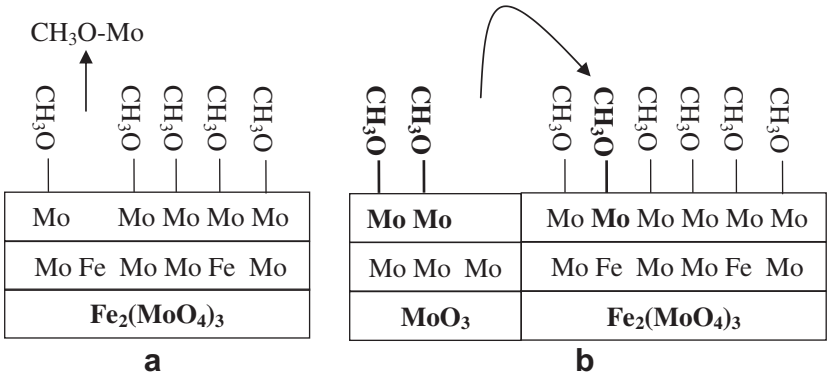

Fig. 13. Schematic representation of catalytic reaction occurring on (a) stoichiometric $Fe_2(MoO_4)_3$ and (b) iron molybdate catalysts with excess MoO_3.

4.6. Synergy between bulk MoO_3 and $Fe_2(MoO_4)_3$ phases

The increase in catalytic performance of bulk iron molybdate catalysts containing excess MoO_3 has been attributed to the contact synergy between excess MoO_3 and $Fe_2(MoO_4)_3$ phases [56,57]. The catalytic activity of bulk $Fe_2(MoO_4)_3$ phase, however, is comparable with or without the presence of excess MoO_3 and the TOF values are almost indistinguishable (see Table 2). The only difference resulting from the presence of excess MoO_3 is the increase in HCHO selectivity (see Table 2). The increase in HCHO selectivity is a consequence of the excess MoO_3 supplying surface MoO_x species that cover up exposed surface FeO_x sites responsible for the formation of acid catalyzed byproducts (DME and DMM). Thus, the current quantitative catalytic investigation has clearly shown that the enhanced catalytic performance is related to the spillover of surface MoO_x redox species [50] that clearly demonstrate that there is no scientific support for the contact synergy model.

According to the remote control model, the excess MoO_3 would play the role of an oxygen donor, which dissociates the gas phase oxygen to atomic oxygen, that is supplied to the acceptor $Fe_2(MoO_4)_3$ phase for methanol oxidation to formaldehyde. Firstly, the studies with the model supported MoO_3/Fe_2O_3 monolayer catalyst demonstrate that the presence of either crystalline MoO_3 or $Fe_2(MoO_4)_3$ are not required for good catalytic performance. Secondly, the current study has shown that the crystalline $Fe_2(MoO_4)_3$ phase rapidly supplies bulk lattice oxygen to the catalytic active surface sites and is able to maintain the surface redox sites in their oxidized state for methanol oxidation (see Fig. 11). Crystalline MoO_3, however, can only sluggishly supply bulk lattice oxygen to the surface and maintain the surface sites in their oxidized state (see Fig. 12). Consequently, the crystalline MoO_3 phase can not be a source of atomic oxygen for the bulk $Fe_2(MoO_4)_3$ phase. Furthermore, the surface sites of the bulk $Fe_2(MoO_4)_3$ phase are fully oxidized and, thus, would not benefit by the supply of additional oxygen from the crystalline MoO_3 phase if this mechanism were operative. This conclusion is further supported by elegant isotopic $H_2{}^{18}O$ Raman studies with MoO_3 and $Fe_2(MoO_4)_3$ catalysts that found that while the bulk MoO_3 lattice remains unchanged the bulk $Fe_2(MoO_4)_3$ lattice readily exchanges its lattice oxygen [10]. These studies clearly demonstrate that there is no scientific basis for the remote control model.

5. Conclusions

The origin for the increase in methanol oxidation steady-state activity of bulk iron molybdate catalysts upon the addition of excess MoO_3 was investigated with LEIS, Raman, IR, temperature programmed CH_3OH-IR and CH_3OH-TPSR spectroscopy as well as steady-state reaction studies.

Chemisorption of methanol on Fe_2O_3 yielded both intact surface CH_3OH^* and a smaller amount of surface CH_3O^* species. The intact surface CH_3OH^* species are responsible for appearance of CH_3OH in the gas phase and the surface CH_3O^* species are responsible for production of DME from Fe_2O_3. The same two surface intermediates are also present on the bulk iron molybdate catalysts (stoichiometric and excess MoO_3), and both form HCHO as the gas phase reaction product. Bulk MoO_3 also yields HCHO as the primary reaction product. Thus, formation of HCHO during methanol oxidation requires the presence of surface MoO_x sites, which is the dominant active redox component in bulk iron molybdate catalysts.

The number of redox catalytic active sites is low for bulk MoO_3 since only the edge planes of this platelet morphology are active. Formation of bulk $Fe_2(MoO_4)_3$, however, transforms the anisotropic morphology of MoO_3 to an isotropic morphology where all the exposed planes are catalytically active. This results in greater than a sixfold increase in number density of redox catalytic active sites. A further increase in number density of redox catalytic active sites is found in the presence of excess crystalline MoO_3 since exposed acidic FeO_x sites become covered by surface MoO_x species from the additional MoO_3.

The role of surface MoO_x species was also examined with a model monolayer supported MoO_3/Fe_2O_3 catalyst where crystalline MoO_3 and $Fe_2(MoO_4)_3$ phases are absent. The catalytic performance of the supported MoO_3/Fe_2O_3 catalyst was found to be comparable to that of the bulk iron molybdate catalysts with excess MoO_3. Consequently, the origin of enhanced activity of excess MoO_3 in bulk iron molybdate catalysts is associated with the formation of a surface MoO_x monolayer, which represents the catalytic active sites, and is continuously replenished by the excess crystalline MoO_3 phase.

The methanol oxidation reaction over the bulk iron molybdates proceeds via a Mars–van Krevelen mechanism employing bulk lattice oxygen, which is replenished by gas phase molecular O_2. The transport of bulk lattice oxygen to the surface of crystalline MoO_3 phase is significantly slower. This indicates that there is no contact synergy mechanism operating between the crystalline MoO_3 and $Fe_2(MoO_4)_3$ phases. As mentioned above, the enhanced catalytic performance is a consequence of the formation of a monolayer of surface MoO_x species on the $Fe_2(MoO_4)_3$ phase by the excess crystalline MoO_3 phase.

Acknowledgments

Financial support of this research was provided by the US Department of Energy-Basic Energy Sciences (Grant DE-FG02-93ER14350) and is gratefully acknowledged. The authors would like to acknowledge the contributions of Sascha Heikens and Inga Ellmers for carrying out the LEIS measurements at Ruhr University and Chris J. Keturakis of Lehigh for obtaining the *in situ* IR measurement of the dehydrated supported 2.3% MoO_3/Fe_2O_3 catalyst while in the lab of Prof. Marcos Daturi at Laboratoire de Catalyse et Spectrochimie, Caen, France.

Appendix A. Supplementary material

Supplementary data associated with this article can be found, in the online version, at doi:10.1016/j.jcat.2010.07.023.

References

[1] H. Adkins, W.R. Peterson, J. Am. Chem. Soc. 53 (1931) 1512.
[2] A.P.V. Soares, M.F. Portela, A. Kiennemann, Catal. Rev. Sci. Eng. 47 (2005) 125.
[3] C.G. Hill, J.H. Wilson III, J. Mol. Catal. 63 (1990) 65.
[4] R.P. Groff, J. Catal. 86 (1984) 215.
[5] L.J. Burcham, L.E. Briand, I.E. Wachs, Langmuir 17 (2001) 6175.
[6] Y. Okamoto, F. Morikawa, K. Oh-Hiraki, T. Imanaka, S. Teranishi, J. Chem. Soc. Chem. Commun. (1981) 1018.
[7] S.K. Bhattacharyya, K. Janakiram, N.D. Ganguly, J. Catal. 8 (1967) 128.
[8] C.J. Machiels, A.W. Sleight, in: H.F. Barry, Philip C.H. Mitchell (Eds.), Chemistry and Uses of Molybdenum, Proc. of the 4th Int. Confer., Ann Arbor, MI, 1982, Climax Molybdenum Co., Michigan, 1982, p. 411.
[9] M.P. House, A.F. Carley, M. Bowker, J. Catal. 252 (2007) 88.
[10] C.J. Machiels, U. Chowdhry, A.W. Sleight, 186th Nat. Meet. Amer. Chem. Soc., Div. of Petro. Chem., Washington, DC, 28 August–2 September 1983, Washington, DC, 1983, p. 1293.
[11] M.P. House, A.F. Carley, R. Echeverria-Valda, M. Bowker, J. Phys. Chem. C 112 (2008) 4333.
[12] U. Chowdhry, A. Ferretti, L.E. Firment, C.J. Machiels, F. Ohuchi, A.W. Sleight, R.H. Staley, Appl. Surf. Sci. 19 (1984) 360.
[13] W.E. Farneth, F. Ohuchi, R.H. Staley, U. Chowdhry, A.W. Sleight, J. Phys. Chem. 89 (1985) 2493.
[14] B. Delmon, in: H.F. Barry, Philip C.H. Mitchell (Eds.), Chemistry and Uses of Molybdenum, Proc. 3rd Int. Confer., Louvain-la-Neuve, Belgium, 1979, MI, 1979, p. 73.
[15] U.S. Ozkan, G.L. Schrader, J. Catal. 95 (1985) 120.
[16] U.S. Ozkan, G.L. Schrader, Appl. Catal. A 23 (1986) 327.
[17] U.S. Ozkan, R.C. Gill, M.R. Smith, J. Catal. 116 (1989) 171.

[18] B. Delmon, G.F. Froment, Catal. Rev. Sci. Eng. 38 (1996) 69.
[19] D. Martin, P. Kaur, D. Duprez, E. Gaigneaux, P. Ruiz, B. Delmon, Catal. Today 32 (1996) 329.
[20] J.M. Tatibouët, Appl. Catal. A 148 (1997) 213.
[21] M. Badlani, I.E. Wachs, Catal. Lett. 75 (2001) 137.
[22] L.E. Briand, A.M. Hirt, I.E. Wachs, J. Catal. 202 (2001) 268.
[23] W.L. Holstein, C.J. Machiels, J. Catal. 162 (1996) 118.
[24] I.E. Wachs, L.E. Briand, US Patent 6 037 290, Lehigh University, 2000.
[25] I.E. Wachs, L.E. Briand, US Patent 6 331 503, Lehigh University, 2001.
[26] K. Routray, L.E. Briand, I.E. Wachs, J. Catal. 256 (2008) 145.
[27] M. Watanabe, D.W. Ackland, C.J. Kiely, D.B. Williams, M. Kanno, R. Hynes, H. Sawada, JEOL News 41 (2006) 2.
[28] F.D. Hardcastle, I.E. Wachs, J. Raman Spectrosc. 21 (1990) 683.
[29] H. Tian, I.E. Wachs, L.E. Briand, J. Phys. Chem. B 109 (2005) 23491.
[30] M.A. Vuurman, I.E. Wachs, J. Mol. Catal. 77 (1992) 29.
[31] Q. Xu, G. Jia, J. Zhang, Z. Feng, C. Li, J. Phys. Chem. C 112 (2008) 9387.
[32] E. Söderhjelm, M.P. House, N. Cruise, J. Holmberg, M. Bowker, J.-O. Bovin, A. Andersson, Top. Catal. 50 (2008) 145.
[33] E.L. Lee, I.E. Wachs, J. Phys. Chem. C 111 (2007) 14410.
[34] G. Mestl, T.K.K. Srinivasan, Catal. Rev. Sci. Eng. 40 (1998) 451.
[35] H. Hu, I.E. Wachs, S.R. Bare, J. Phys. Chem. 99 (1995) 10897.
[36] I.E. Wachs, Catal. Today 27 (1996) 437.
[37] A. Glisenti, G. Favero, G. Granozzi, J. Chem. Soc. Faraday Trans. 94 (1998) 173.
[38] W.E. Farneth, R.H. Staley, A.W. Sleight, J. Am. Chem. Soc. 108 (1986) 2327.
[39] K. Routray, G. Deo, AIChE J. 51 (2005) 1733.
[40] H. Liu, E. Iglesia, J. Catal. 223 (2004) 161.
[41] G. Deo, I.E. Wachs, J. Catal. 146 (1994) 323.
[42] I.E. Wachs, R.J. Madix, J. Catal. 53 (1978) 208.
[43] I.E. Wachs, J.-M. Jehng, W. Ueda, J. Phys. Chem. B 109 (2005) 2275.
[44] L.J. Burcham, M. Badlani, I.E. Wachs, J. Catal. 203 (2001) 104.
[45] E.L. Lee, I.E. Wachs, J. Phys. Chem. C 112 (2008) 20418.
[46] J. Handzlik, P. Sautet, J. Phys. Chem. C 112 (2008) 14456.
[47] J. Handzlik, Chem. Phys. Lett. 469 (2009) 140.
[48] J. Haber, E. Lalik, Catal. Today 33 (1997) 119.
[49] E.M. McCarron III, A.W. Sleight, Polyhedron 5 (1986) 129.
[50] C.-B. Wang, Y. Cai, I.E. Wachs, Langmuir 15 (1999) 1223.
[51] C.J. Machiels, U. Chowdhry, W.T.A. Harrison, A.W. Sleight, ACS Symposium Series, vol. 279, 1985, p. 103.
[52] F. Trifiro, G. Caputo, P.L. Villa, J. Less-Common Met. 54 (1977) 373.
[53] H. Zhang, J. Shen, X. Ge, J. Solid State Chem. 117 (1995) 127.
[54] N. Burriesci, F. Garbassi, M. Petrera, G. Petrini, N. Pernicone, Stud. Surf. Sci. Catal. 6 (1980) 115.
[55] S.D.M. Jacques, O. Leynaud, D. Strusevich, A.M. Beale, G. Sankar, C.M. Martin, P. Barnes, Angew. Chem. Int. Ed. 45 (2006) 445.
[56] L.E. Cadus, Y.L. Xiong, F.J. Gotor, D. Acosta, J. Naud, P. Ruiz, B. Delmon, Stud. Surf. Sci. Catal. 82 (1994) 41.
[57] E. Soderhjelm, M.P. House, N. Cruise, J. Holmberg, M. Bowker, J.-O. Bovin, A. Andersson, Top. Catal. 50 (2008) 145.